DISCRETE STRUCTURAL MODELS OF COMBAT AIRCRAFT AND THEIR APPLICATION IN AEROELASTIC ANALYSES PERFORMED IN CAE SOFTWARE

Aleksander Olejnik **Robert Rogólski**

Military University of Technology
Faculty of Mechatronics and Aeronautics

aolejnik@wat.edu.pl rrogolski@wat.edu.pl

Abstract. The paper is devoted to combat aircraft structure modelling and application of finite element models (FEM) in some numerical aeroelastic analyses. FEM models of currently operated in Polish Air Force fighters MiG-29 and F-16 C are demonstrated with consideration to mass and stiffness distribution. The methods used in model-correctness verification are talked over briefly. The stationary flight loads were determined with taking into account aerodynamic and mass forces; the load size and distribution over airframe were assessed too. The model static and dynamic analyses were performed for certain mission variants – static deformations, structure strength, free vibrations, flutter velocities were calculated. The examples of results presented in paper are: displacement and strength distribution, normal modes and frequencies. The results illustrating external store effect on static and dynamic structure parameters are inserted too. The whole project cycle including FEM preprocessing, numerical analyses and result postprocessing was carried out taking advantages of advanced CAE software: UG NX and MSC.Software (Patran, MD Nastran).

Keywords. FEM, aeroelasticity

1 Introduction

For several years in Institute of Aviation Technology of Faculty of Mechatronics and Aeronautics MUT the researches are being performed, of which the main purpose is to define parameters and to investigate structural characteristics of some type of aircraft run in Polish Air Force (PAF). In that research process some characteristic quantities are being determined which concern static and dynamic airplane properties – essential features from the point of view of structural aeroelasticity. To determine values and functional relations between such parameters like: structure component masses, mass moments of inertia, aerodynamic loads, displacements, stresses, normal modes frequencies, divergence or flutter critical airspeed and others – it is very useful in many aspects. In operational aspect – it allows to recognize real aircraft operating conditions and unequivocally to estimate the limiting states, which are not to exceed for user (ultimate velocities, angles of attack, load factors and responding to them extreme displacements, stresses or vibration levels). In that meaning the precise design, structural and performance data (obtained from tests or analysis) is quite significant in future plans regarding airframe main repair or its probable backfit. As far as any backfit is concerned parameters of factory construction are then the reference base for those of modified piece. Scientific aspect of whole undertaking is important as well. To recognize performance, aerodynamic, structural, operational etc. parameters means to be able to define optimization models (objective function, proper criteria), which in turn allows to type structural parameters (design variables) best justified for some mission assumptions (constraints).

The researches carried out for MiG-29 and F-16C structure quality evaluation are based both on experimental and simulation methods. In that second path the advanced computer tools and techniques are used aiding geometry identification and recording, structure and aerodynamics modeling and of course specific problems solutions. In this paper some methodics of developing mass-stiffness finite element models is demonstrated, useful in aircraft aeroelastic analysis. Some selected examples of numerical structure analysis of MiG-29 and F-16C aircraft are discussed, both in area of statics and dynamics. MSC.Software package was used as advanced CAE tool set – Patran fulfilled the role of pre- and postprocessor and MD Nastran was run as a numeric processor for statics, normal modes and flutter cases.

The material in paper was elaborated within a framework of two research projects sponsored form the fund of Polish Ministry of Science and Higher Education. In years 2006-2008 – project entitled: *Structure and Aerodynamic Modelling of the Combat Aircraft Operated in Polish Air Force for Flutter Analysis with Consideration of Airframe Heavy Repairs* [18], and then in years 2010-2013 project entitled: *Identification of Integrated Aeroelastic Models of Combat Aircraft Aided by Reverse Engineering Techniques*, which is still being realized.

2 Aircraft structure discretisation in CAE preprocessor

In investigation of aircraft lifting structure with use of simulation techniques the main undertaking is to prepare proper and correct discrete virtual model, which could be applied then in Finite Element Analysis (FEA). Aircraft structure modeling is very time- and labour-consuming process, particularly by the assumption the model should simulate both mass and stiffness properties as well as those features are distributed in real object. In whole cycle of MiG-29 and F-16 FEM model generation with use of virtual CAD/CAE environment (UX NX, Patran) the following development stages could be distinguished:

- geometry model recovering in CAD environment with application of RE tools,
- FE mesh generation (one- and two-dimensional elements for thin-walled structure like an airframe),
- structure material identification (material constants: E, G, ρ, ν),
- physical (material) properties input for specified elements,
- locating lumped mass elements imitating on-board equipment and cargo items,
- definition of hinge connections (RBE) and controls artificial stiffness (CELAS) for movable surfaces,
- model boundary conditions responding to free object with possibility of symmetric, antisymmetric or arbitrary deformation modes.

So to develop FEM model properly it is necessary to identify geometric, structural, mass, and material parameters of real object. The whole that process referring to MiG-29 aircraft was reported in [18].

2.1 Geometry modeling process

Within the framework of the task formulated as the airframe geometry recreation in the advanced CAD environment the following activities were performed:

1) geodetic measurement of airframe body (about 1000 measured points),
2) point coordinates input into the CAD programme space,
3) generating definitive cross-curves using the point sets collected in measurement body-sections,
4) aircraft surface body generating.

Levelling measurements in pre-defined body sections were performed. About 1000 outline points were identified.

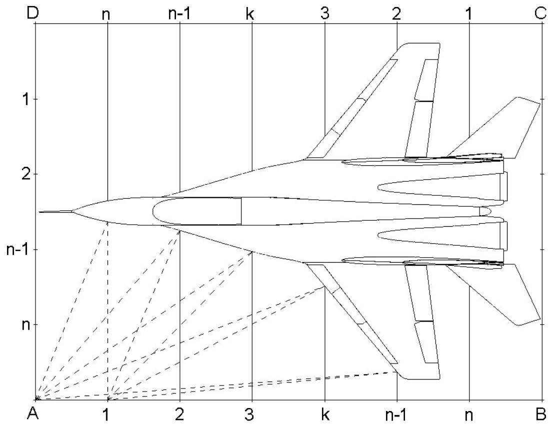

Fig. 1 Reference grid of coordinates for levelling airframe points in pre-defined body sections.

The geometric model was elaborated in UG. The process of the point coordinates input was automated thanks to translating procedures defined in the user-system interactive language called GRIP. The successive stages of the geometry modelling are shown in Fig. 2 The example virtual recreation of inner structure parts is shown in Fig. 3.

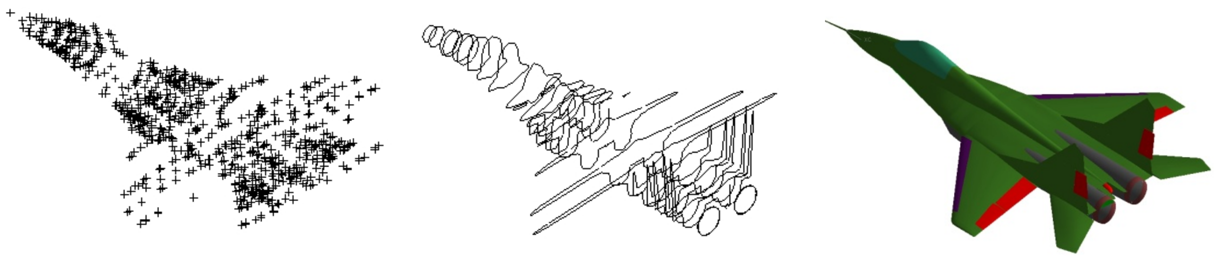

Fig. 2 The successive stages of the airframe CAD geometry (UG): measurement points, cross-section defining curves, final surface model after the applying the smoothing procedures

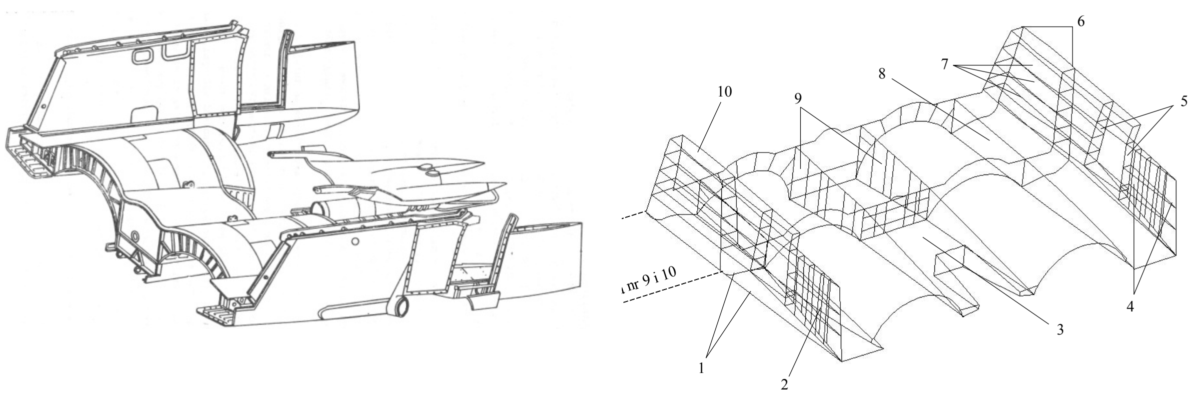

Fig. 3 Rear fuselage assembly – structural scheme [21] and CAD model parts: 1-stabilizer support knots , 2-fairing, 3-parachute bay, 4-division wall, 5-fin posts, 6-fin support knots, 7-ribs, 8, 9-longitudinal walls, 10-root rib.

Geometry measurements of F-16 airframe were carried out with application of ultra advanced RE tools. Two non-tactile high precision systems were used:
- portable optical scanner ATOS II Triple Scan,
- portable fotogrametric system TRITOP equipped with digital photo-camera and encoding markers.

Fig. 4 ATOS II Triple Scan in use – scanning points on wing lower skin.

The results obtained from the scanning measurement with tool like ATOS II Triple Scan is so called cloud of points – about 35 mln points of which coordinates are identified by measuring tool. In triangulation process the cloud is transformed into the triangle mesh. On that mesh geometry definitive curves were generated in GOM ATOS Professional software, then smoothed into B-splines. The final surface model were prepared in UG NX – the assembly of joined smoothed surfaces. In Fig. 5 the development stages of virtual geometry recreation are shown.

Both in case of Mig-29 and F-16 geometry modeling outlines of inner structure thin-walled parts (like frames, ribs, walls) were generated as products of intersection of crosswise or longitudinal planes with specific component surface geometry (Fig. 3 and 6)

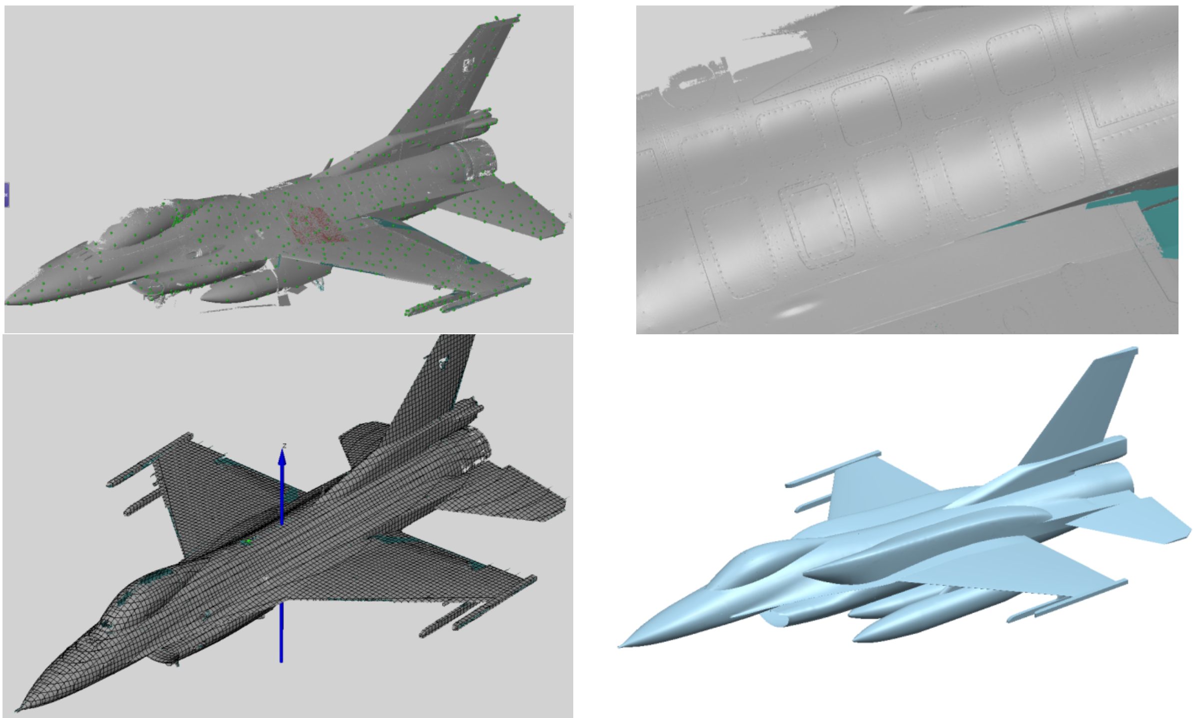

Fig. 5 Successive stages of surface geometric F-16 model recreation.

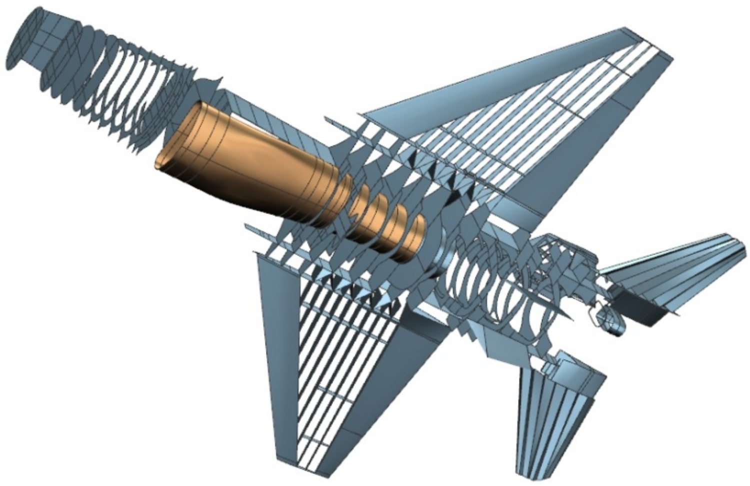

Fig. 6 Surfaces of inner thin-walled parts of F-16C airframe.

2.2 Structural data acquisition

Industrial technology documentation of both analyzed aircraft is of course unavailable for user. But to develop FEM structure except of geometry CAD model many other data are necessary, like the following:

- location and dimension of inner structural parts,
- identification of structure materials – kinds of alloys or types of composites and material constants,
- structural masses of airframe components,
- location and masses of on-board nonstructural elements – generally equipment and cargo,
- masses of suspended elements (storages, bombs, missiles, tanks),
- movable surfaces hinge and controls locations .

To identify the above data the following sources were studied:

- real aircraft in military units and aircraft works,
- oparation manuals and instructions of both aircraft [19-24],
- heavy repair documentation of MiG-29 from Military Aircraft Works No 2 [8, 9, 15],
- accessible monographs and publications [2, 6].

Distributions of thin-walled internal model elements were taken from schemes and illustrations available in manuals. There are two examples below: scheme of internal wing structure [21] and lay-out of fuselage frames [19].

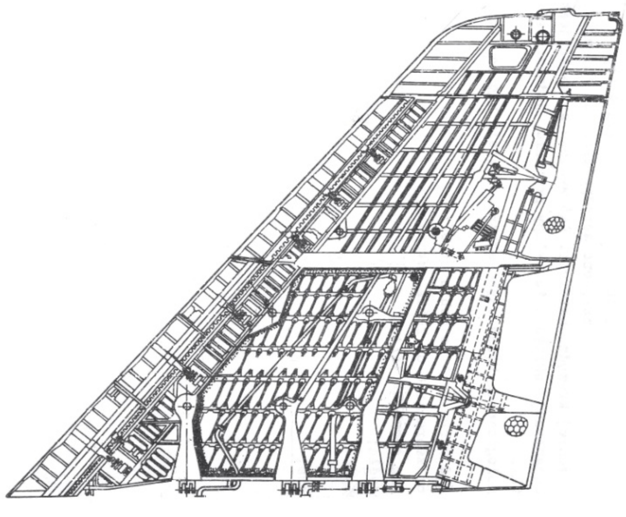

Fig. 7a Scheme of internal wing structure of MiG-29 aircraft [21]

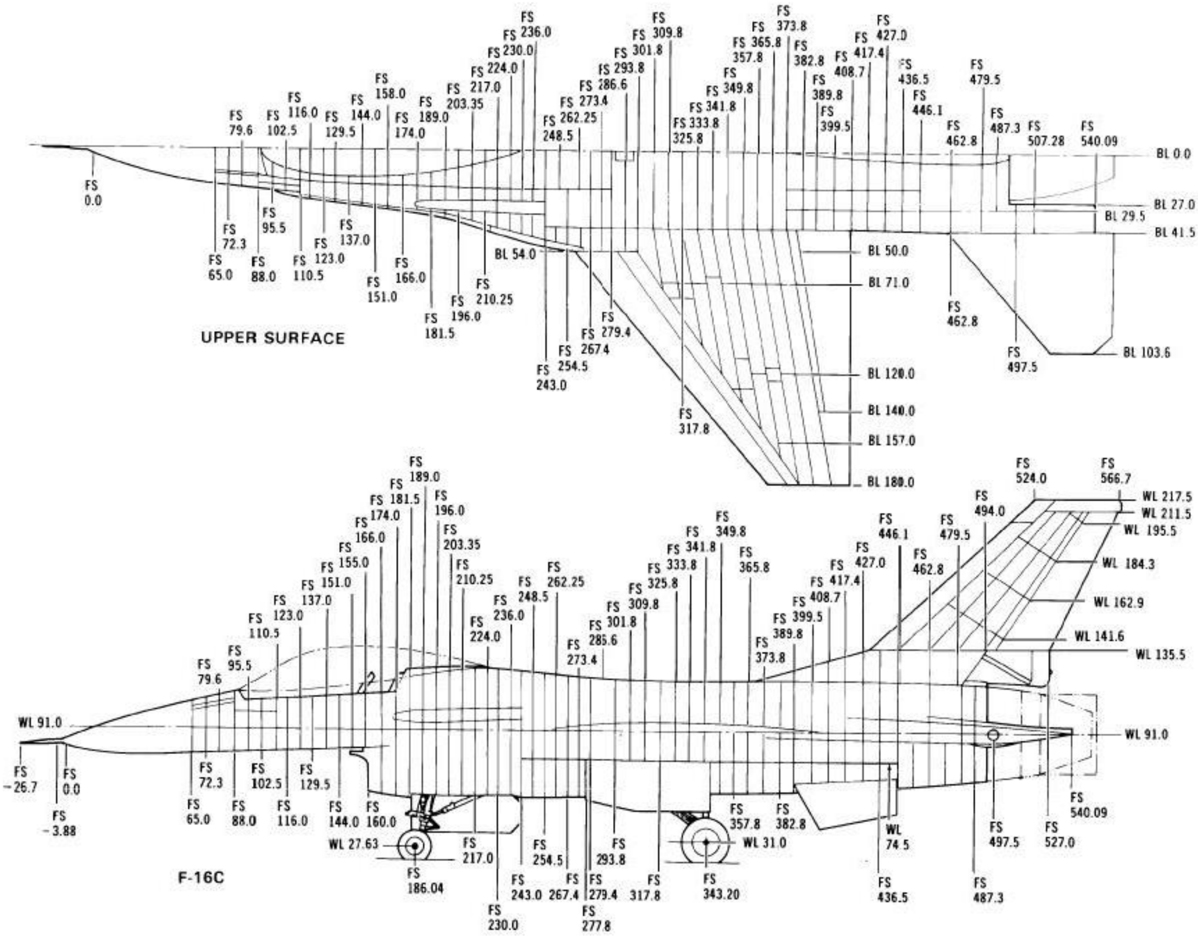

Fig. 7b Frame stations lay-out of F-16 C [19].

Regarding structural data, in both cases the catalogues of stiffening element cross-section drawings were prepared. The drawings of frame stiffeners distribution were prepared as well what allows to match proper section with proper elements. Material symbols were identified in both catalogues too. In case when it was impossible to find the real material data the substitute material data – most probable for specific part – were taken from [7].

Kształt	Nazwa	Umieszczenie na płatowcu [nr / nr rys.]	Materiał	Wymiary [mm]		
				h	a	b
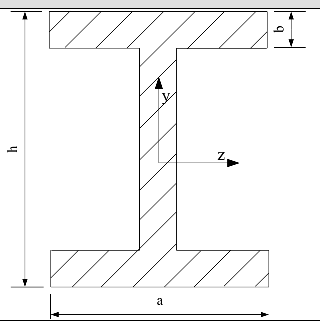	żebro nr 3	8 / 4.9a	Pa 30 (AK4-1)	189,0	61,8	4,0
	żebro nr 4			181,1	66,2	4,0
	żebro nr 8			140,3	64	7,8
	dźwigar nr 1	3 / 4.9a	WT 4-1	206,6	70,5	6,3

Fig. 8 The part of the catalogue containing cross-sections characteristics of internal elements of MiG-29 airframe.

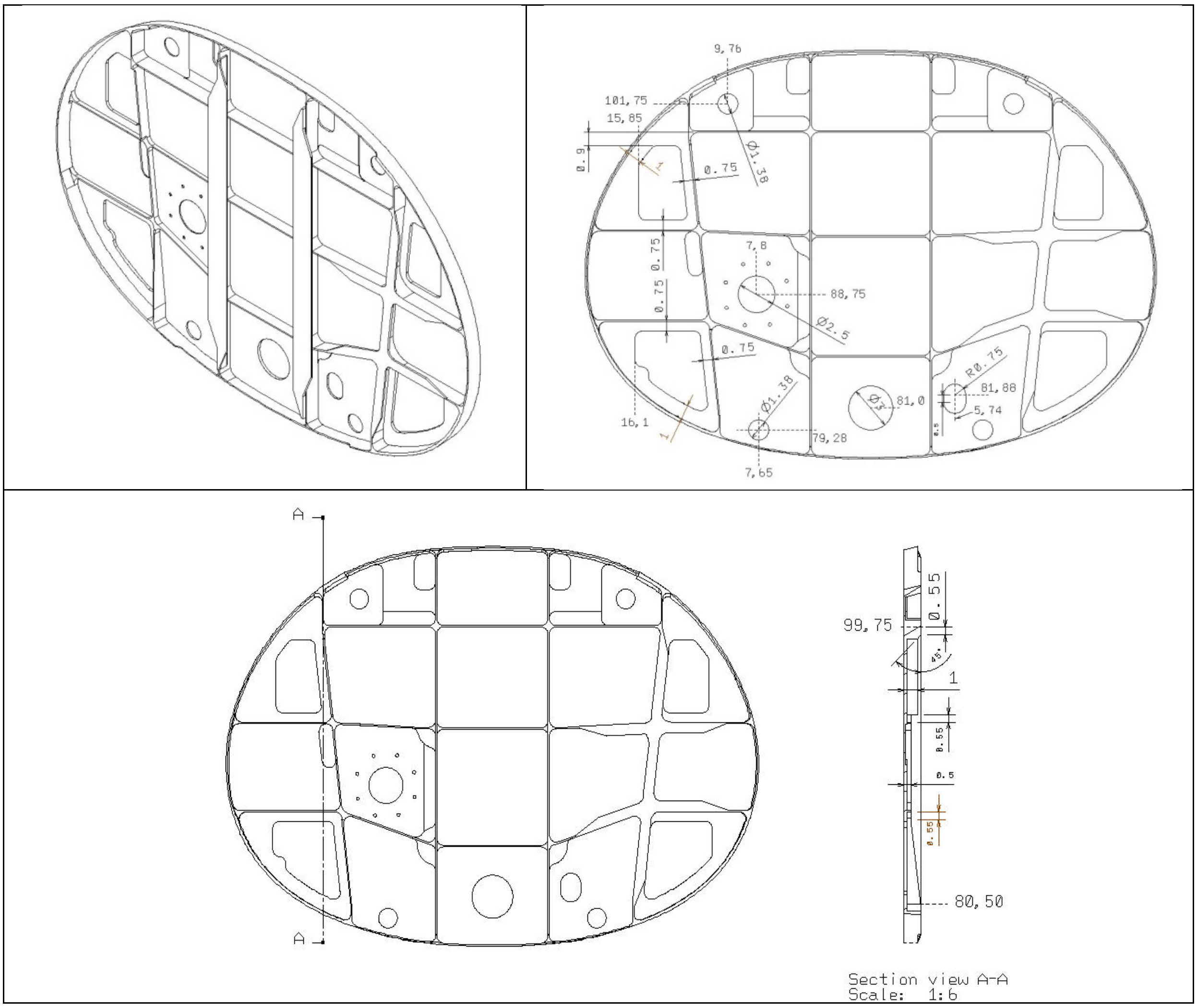

Fig. 9 Distribution of stiffeners and their dimensions in frame FS-65 of F-16 C

The list of non-structural on-board elements was prepared for MiG-29 aircraft. The masses of power plants, fuel and powering systems units, and avionic devices were identified. The geometric centres of those parts were estimated – singular mass points were taken as approximate mass centres. Some part of that data sheet was presented in the table 1. The analogous list is just being prepared for F-16C aircraft.

Tab. 1 Part of the equipment-mass data list (airframe power units); in the following columns: element name, symbol, coordinates of the element middle and a number of the location node, mass, quantity and remarks.

No.	Element name	Symbol	Coordinates / grid label	Mass	Remarks
55.	Hydraulic distributor	773300	[7140, 0, 245] 100035	3,1	together 5,4 kg, frame 3D-4, recess of the front landing gear
56.	Hydraulic distributor	773900		1,2	
57.	Control valve RDM	773500		1,1	
58.	Control unit	AU-46-06	[7140, 0, 288] 100034	4,8	2
59.	Acuator-strut of front undercarriage leg		[5490, 0, -94] 100031	18,7	1
60.	Acuator-strut of rear undercarriage leg		[10895, -1350, 41] 100029 [10895, 1350, 41] 100030	18	2 (r/l)

2.3 Finite element modelling

Discrete structural models of both aircraft were developed on surface mesh. They consists of shell elements (triangles or quadrilaterals) and one-dimensional elements (rods and bars) which are added to stiffen the internal structure [16]. The control surfaces like rudders, stabilizers and ailerons are movable thanks to applying hinge connections made of *RBE* rigid elements and elastic *CELAS* elements. Material properties of elements were established according to material distribution of the real airframe structure. An example of the material distribution in the partial model is shown in the Fig. 11.

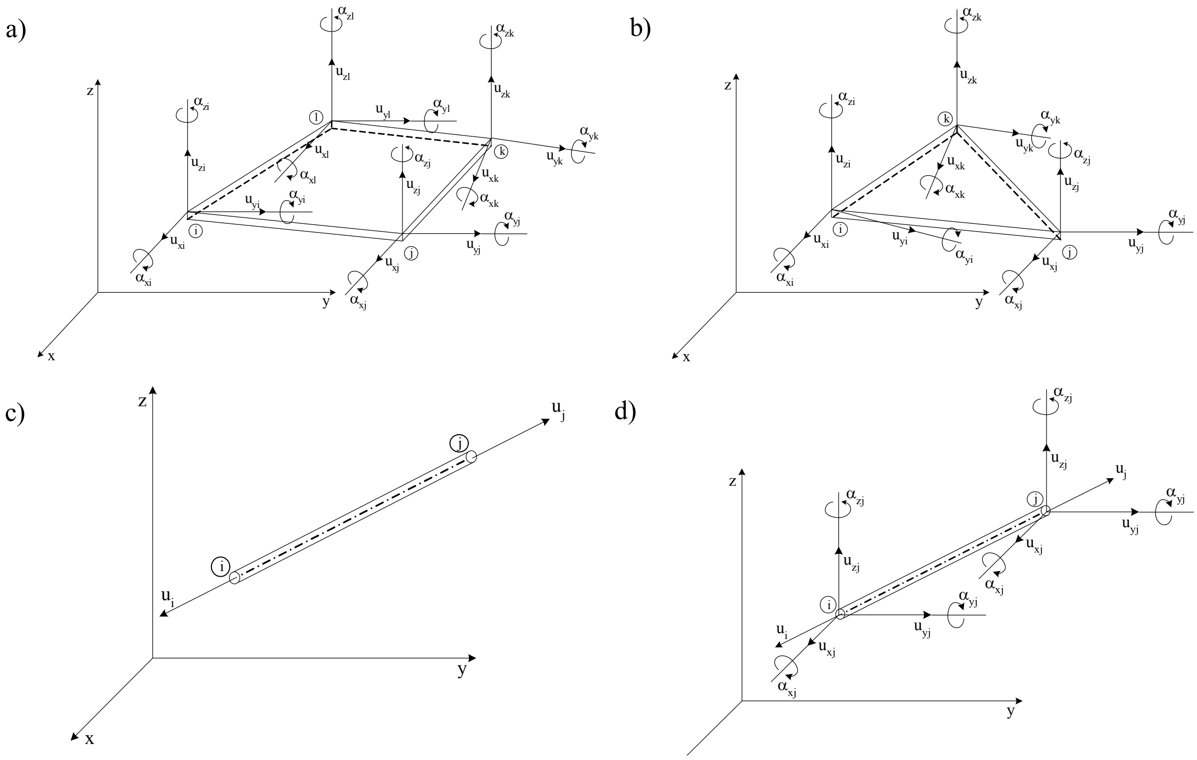

Fig. 10 Finite elements applied in the aircraft discrete model: a) quadrilateral element *CQUAD4*, b) triangle element *CTRIA3*, c) rod element *CROD*, d) constant-section beam element *CBAR*.

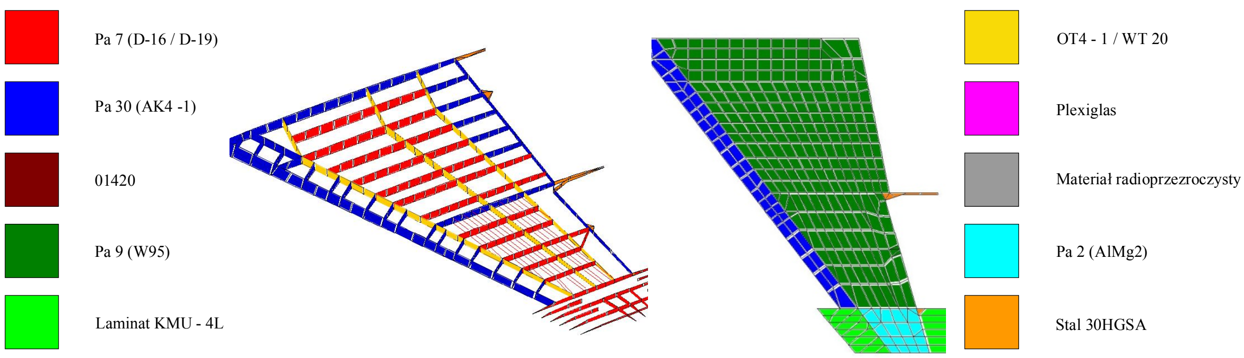

Fig. 11 Airframe structure materials and an example of their distribution (MiG-29 wing structural model).

Airframe virtual structures are shown in Fig. 12 and 13. Up till now the F-16 aircraft model is just only airframe structure but without internal mass elements, therefore it is suitable only for static solutions. But the MiG-29 aircraft model has both stiffness and mass properties completed and is suitable for dynamic solutions either. Structural mass of the model calculated in pre-processor amounted to 5070 kg. The total fixed-equipment mass was estimated for 5046 kg (airframe and power plant units: 3630 kg, armament units: 502 kg, electrical equipment units: 414 kg, radio-electronic equipment blocks: 500 kg). Total model mass amounted finally to 10104 kg, centre of gravity located in 25.8% *MAC.* (Fig. 14). The real empty aircraft mass is 10900 kg so model mass deviation is about 7%.

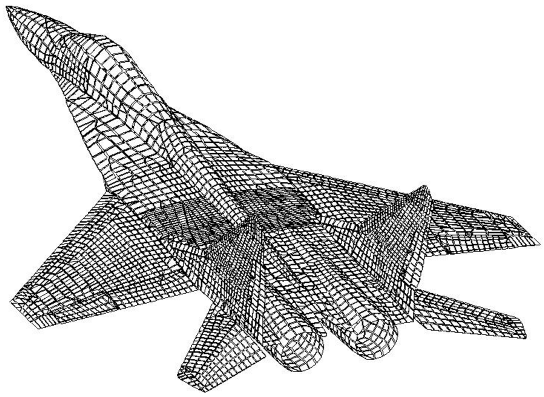

Fig. 12 Discrete structural model of the MiG-29 airframe for FEM analysis.

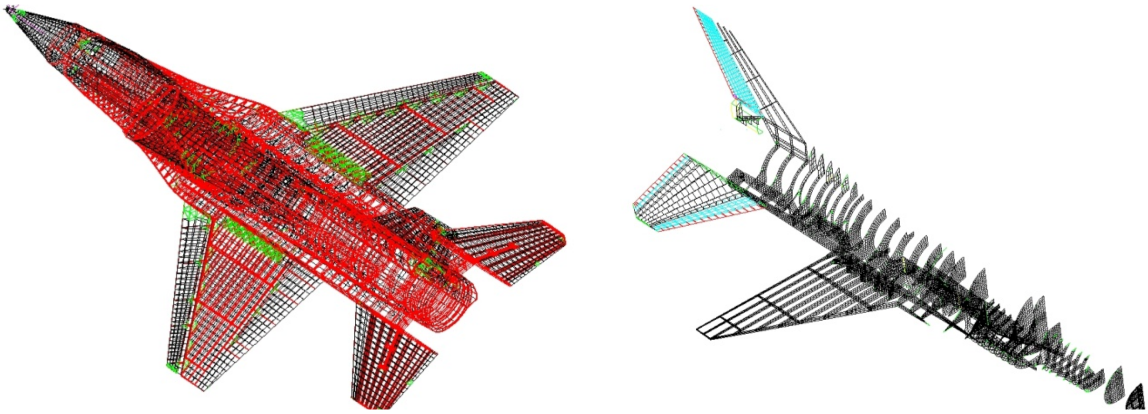

Fig. 13 Discrete structural model of the F-16C airframe – the whole model and inner structure parts.

The first approximations of natural frequencies from the thin-walled FEM structure analysis were quite divergent from those from measured resonance frequencies. Therefore there occurred a necessity to adjust numerical modes to experimental results. Therefore the dynamic reduced two-dimensional model was developed, based on simplified planar geometry. That model was dynamically equivalent towards the previous one. The number of elements was quite small (about 1600), but for fast prediction of dynamic behaviour it was much more convenient and easier for calibration.

The simplified FEM structure is just a two-dimensional shell-beam model. The aircraft lifting surfaces were modelled by quadrilateral shell elements (wings, tail, wing band, fuselage lifting part); whereas the slender nose fuselage part and power plant solids were modelled using equivalent beam elements. The geometry of the plane airframe assemblies in form of the planar surfaces was assumed after projection of lifting surface outlines on their chord planes. The shell element thickness h_{red} was matched in accordance to bendig stiffeness criterion – stiffness in selected segment of base structure cross section must be the same as stiffness in analogous cross section segment of simplified model [3]. Cross sections of base structure are mostly double-T bars (sections of spars and walls) or double-flat bars (lower- and upper-skin sections). Then for the fixed segment width b i and for previously calculated inertia moment of base section segment J_{bas} the reduced element thickness h_{red} could be calculated according to formulae below:

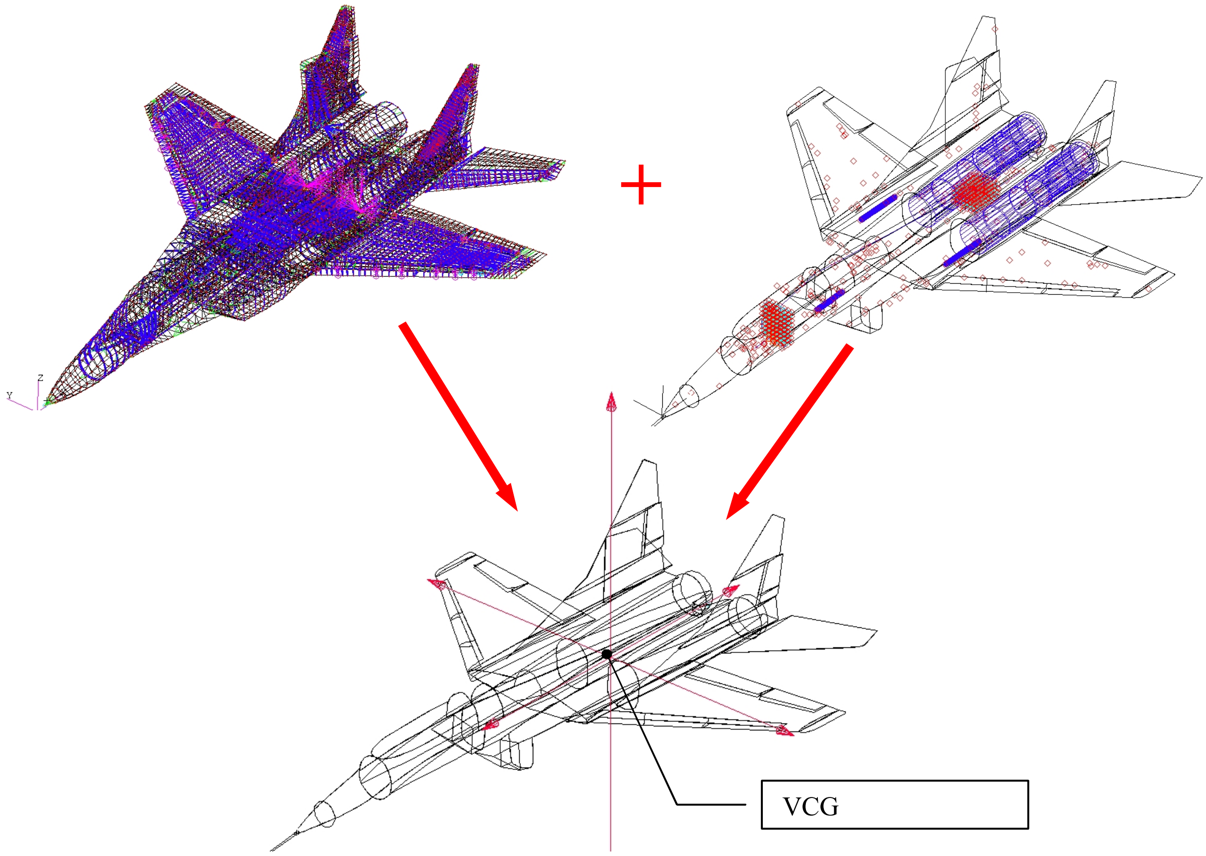

Fig. 14 Aircraft mass model obtained by adding lumped-mass elements to airframe model; *m*=10116 kg, Virtual centre of gravity. located in 25.8% *MAC*.

$$EJ_{bas} = EI_{red} \tag{1}$$

$$I_{bas} = \frac{bh_{red}^3}{12} \Rightarrow h_{red} = \sqrt[3]{\frac{12I_{bas}}{b}} \tag{2}$$

As diameters of beam circular sections were taken medium values estimated on dimensions of two limiting sections of the equivalent slender element. The hypothetical isotropic materials were defined for specified model parts (real structure is made mostly of aluminium alloys). For density estimating the approximate formulas were used that defines density upon dimensions and mass of a lifting structure part (ρ_{ls}) or a slender element (ρ_{sb}):

$$\rho_{ls} = \frac{m_{ls}}{\sum S_i (h_{red})_i} \tag{3}$$

$$\rho_{sb} = \frac{m_{sb}}{\frac{\pi}{4}\left(\overline{D}_{sb}^2 - \overline{d}_{sb}^2\right) l_{sb}} \tag{4}$$

where
S_i – surface of an i-th substitute shell element, $\overline{D}_{sb}$ – medium outer diameter of slender body, $\bar{d}_{sb}$ – medium inner diameter of slender body, l_{sb} – slender body length, m_{ls} – lifting structure mass, m_{sb} – slender body mass.

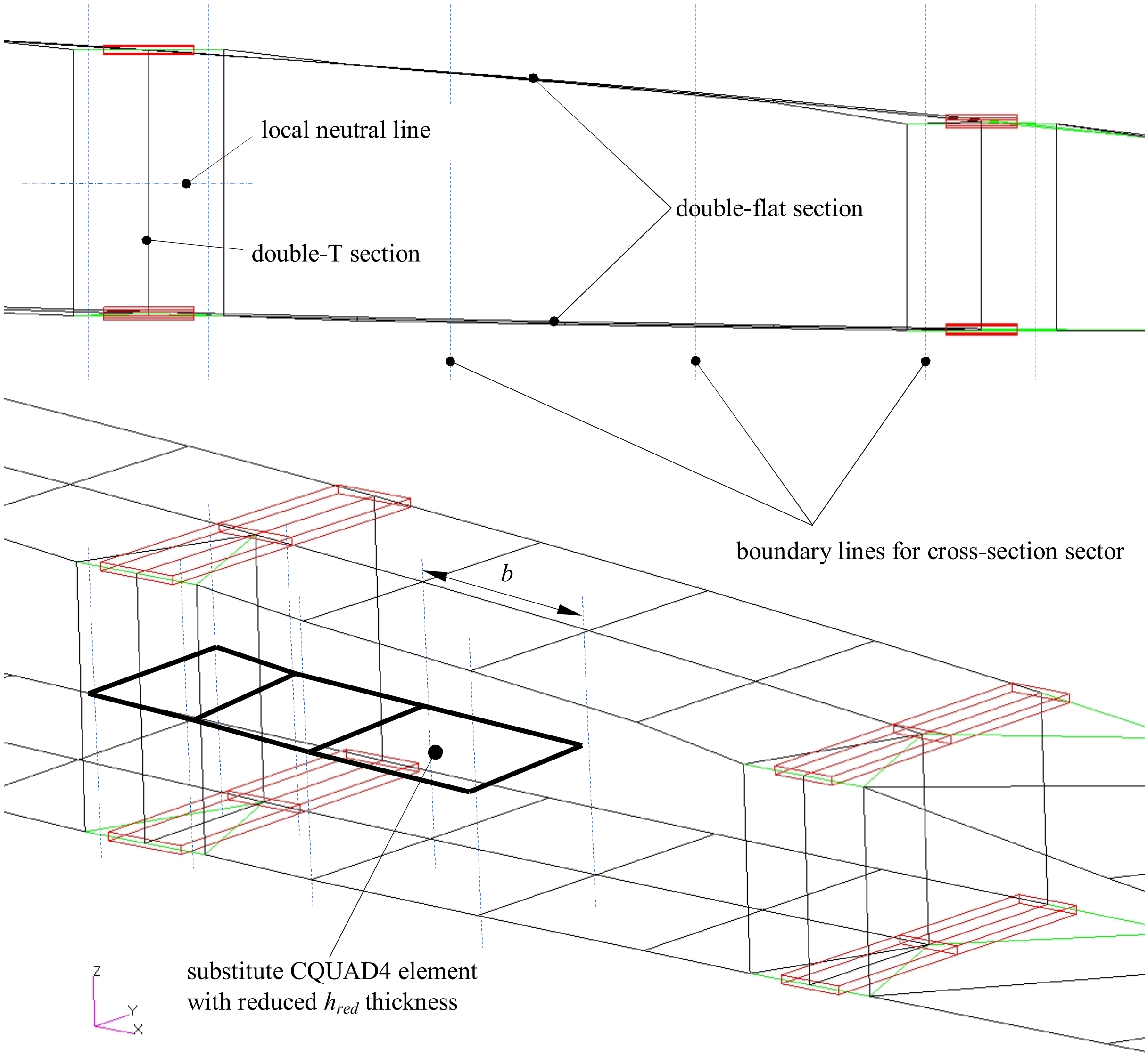

Fig. 15 Method for introducing the substitute one-layer shell model instead of thin-walled 3D structure – as an exemple the pass of close-to-fuselage wing structure was demonstrated.

To estimate structural masses of the airframe some empirical formulas were used approximately determining component masses of fighter structural assemblies [1]. The expressions determine subsequently: wing mass (m_W), tail mass (m_T), fuselage mass (m_F), engine nacelles mass (m_N); all values in anglosaxon units [lb]:

$$m_W = 3.08\left\{\frac{K_{PIV} n m_{TO}}{t/c} * \left[\left(\tan\chi_{LE} - \frac{2(1-\eta)}{\lambda(1+\eta)}\right)^2 + 1.0\right] * 10^{-6}\right\}^{0.593} * \left[(1+\eta)\lambda\right]^{0.89} * \left(S_W\right)^{0.741} \tag{5}$$

$$m_T = 5.4\left\{\frac{K_{PIV} n m_{TO}}{t/c} * \left[\left(\tan\chi_{LE} - \frac{2(1-\eta)}{\lambda(1+\eta)}\right)^2 + 1.0\right] * 10^{-6}\right\}^{0.455} * \left[(1+\eta)\lambda\right]^{0.683} * \left(S_W K_{TAIL}\right)^{0.569} \tag{6}$$

$$m_F = 10.43(K_{INL})^{1.42}(q_{\max} \times 10^{-2})^{0.283} * (m_{TO} \times 10^{-3})^{0.95}\left(\frac{L}{H_F}\right)^{0.71} \quad (7)$$

$$m_N = 0.055 * T_{TO} \quad (8)$$

where:

K_{PIV} –factor depending on wing geometry, n – ultimate load factor, t/c – wing thickness ratio, χ_{LE} – leading edge sweep angle, η – wing taper ratio, λ – wing aspect ratio, S_W – wing surface, K_{TAIL} – factor depending on tail geometry, K_{INL} – factor depending on intake location, q_{max} – maximal dynamic pressure, L – fuselage length, H_F – maximal vertical dimension of fuselage section, T_{TO} – maximal starting thrust.

Masses estimated according to such formulas were compared to the part component masses of the previously developed 3-dimensional model. As the comparing values were rather convergent the masses established as correct were those from the 3-D model but possibly with slight corrections. The mass of power units and on-board equipment was taken into account as so called non-structural mass (*NSM*) added to structural element; it was defined by appropriate density factor – surface density for shell elements [kg/m^2] and linear density for bar elements [*kg/m*]. To establish stiffness constants (*E*, *G*, *v*) of equivalent materials the static model analysis were performed what allowed to compare both models in the same load cases. Structure displacements were determined for applied load distribution responding the D-point of the MiG-29 flight envelope. The separated partial structural models were statically analysed; they were applied fictional but unified boundary conditions and equivalent similar load distributions. For preliminary analysis of each separated structural unit stiffness constants were accepted that were typical for real materials. The sequence of calculations was carried out – for each time constants *E* i *G* were modified. Stiffness constants were acknowledged as proper as output maximal displacements were consistent with maximal displacements of 3-D model (tab. 2).

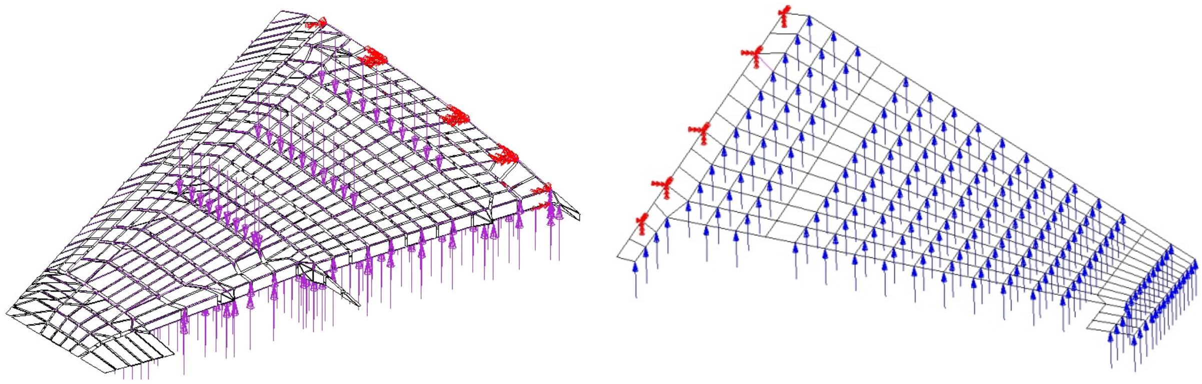

Fig. 16 Thin-walled MiG-29 FEM structure and its simplified model – both with load distributions and boundary conditions (wing example).

Tab. 2 Maximal displacements for statically loaded partial models of MiG-29 structural components.

	Thin-walled FEM	Shell-beam FEM
	u_{max} [mm]	u_{max} [mm]
Wing	129	130
Fin	79,3	79,4
Stabilizer	17,6	17,5
Fuselage	77,1	77,5

As similarity criteria concerning geometry, stiffness and mass were fulfilled the final shell-beam aircraft model was accepted for further dynamical analysis – variant smooth, without a fuel mass (fig. 17). The model mass was estimated at a value of 10905 kg, centre of gravity located in 26.6%*MAC*.

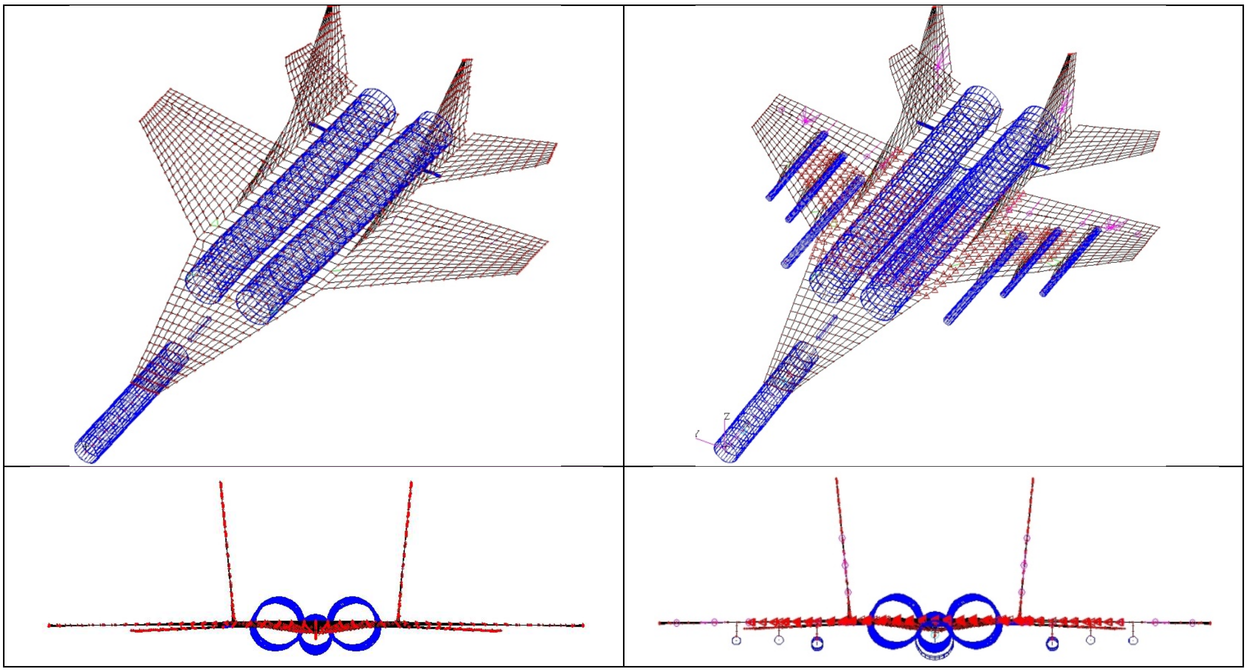

Fig. 17. Shell-beam dynamical model of the MiG-29 aircraft – empty mass and mission configurations (fuel in integral tanks + fuel in under-fuselage tank + 2 missiles R-27 + 4 missiles R-73E).

3 External loads determination and aircraft static analysis

Combat aircraft static analysis comprised load distribution determining and numerical FEM calculations considering solution of the following matrix formula [16]:

$$\mathbf{K} * \mathbf{q} = \mathbf{F} \tag{1}$$

In each analytical subcase load vector matrix **F** resulted from the load factor value and the assumed aerodynamic load and mass distribution (q_a, q_m) Load factors n and specific design velocities were calculated in accordance to expressions stated in aviation regulations MIL-A-8861B (AS).

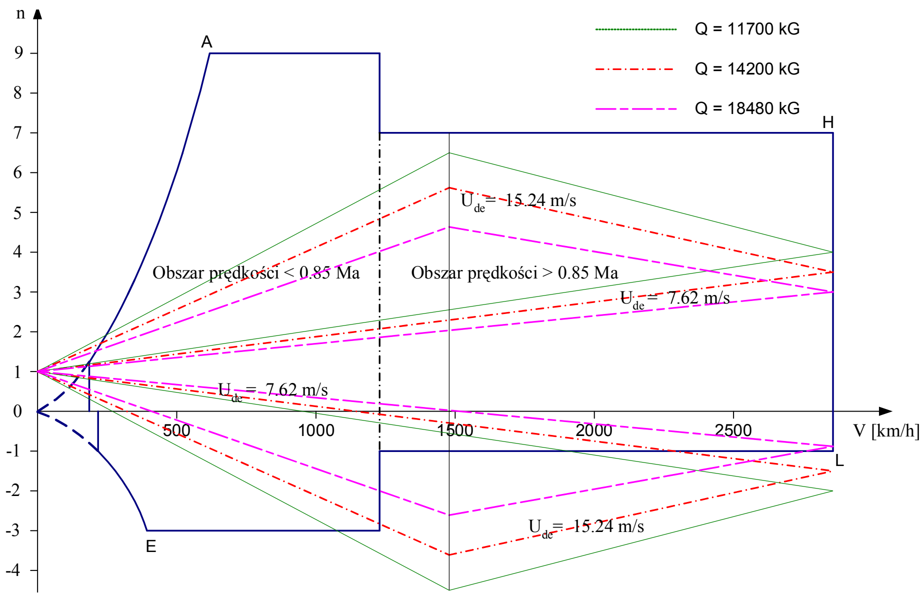

Fig. 17 Flight envelope for maneuvering and gust loads of MiG-29 [according to MIL-A-8861B (AS)].

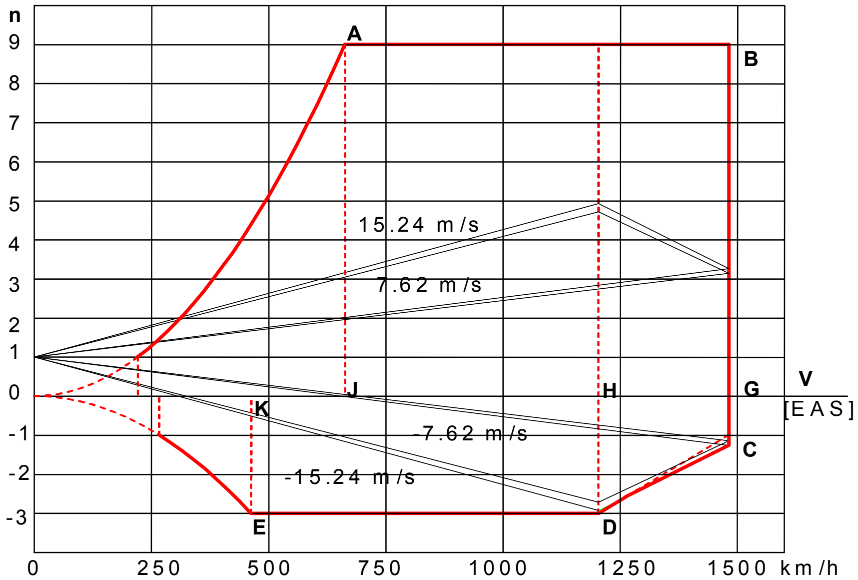

Fig. 18 17 Flight envelope for maneuvering and gust loads of F=16C [according to MIL-A-8861B (AS)].

Scheme of the wing load distribution taken for static analysis is shown in Fig. 19. The simplified chordwise load distribution was assumed – triangular distribution corresponding to pressure load at subsonic velocities and uniform distribution corresponding to load cases at supersonic velocities [5, 25].

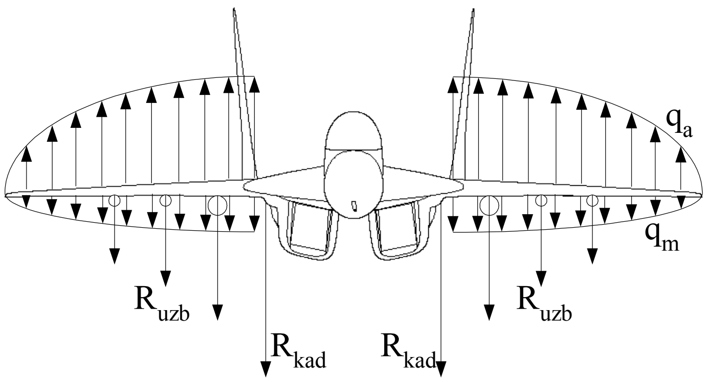

Fig. 19 Simpified aerodynamic spanwise load on MiG-29 airframe

Determining load in simplified way – e.g. basing on wing chord method [4, 5, 17] – it is possible to calculate current aerodynamic or mass loads from the following formulae:

$$q_a = \frac{n_o m g}{S} b(y) \tag{9}$$

$$q_m(y) = \frac{n_o m_{skrz} g}{S} b(y) \tag{10}$$

and the weight of i-th suspension:

$$R_i = n_o m_i g \tag{11}$$

Finally resultant current load at any distance y from the plane of symmetry is calculated as the sum of following terms:

$$q_w(y) = q_a(y) + q_m(y) + \sum R_i(y_i) \tag{12}$$

Specific kinds of maximal wing load – acting usually in root chord section – that means maximal values of transverse force T, bending moment M_g and torsional moment M_S would be calculated from the following integral expressions:

$$T_{\max} = \int_{o}^{l} q_w(y)dy \qquad M_{g-\max} = \int_{0}^{l}\left(\int_{o}^{l} q_w(y)dy\right)dy \qquad M_{s-\max} = \int_{0}^{l}\left[q_w(y)\cdot e(y)\right]dy \tag{13}$$

where l is a wing semi-span and $e(y)$ is a function defining spanwise changing distance between centre of pressure axis and elastic axis. Formulae (13) could be then used to calculate stresses in cross-section – respectively: shear stresses in spar walls, normal stresses in spar flanges and shear stresses in skin of torsion box.

In static analysis of MiG-29 aircraft concentrated forcec from suspended mass element were taken into account. Consideration was given to the dedicated guided missile weapons:

- R–27 missile (230 kg) + laucher unit (71 kg),
- R–73 missile (104,5 kg) + laucher unit (57 kg),
- R–60 missile (45 kg) + laucher unit (32 kg).

Noncombat vehicle mass value for mass load distribution was assumed as 14400 kg what more or less corresponds to mass of full refueled aircraft (only integral tanks) [6]. Sample FEM structure load distributions and resultant stress or displacement distributions are shown in some figures below.

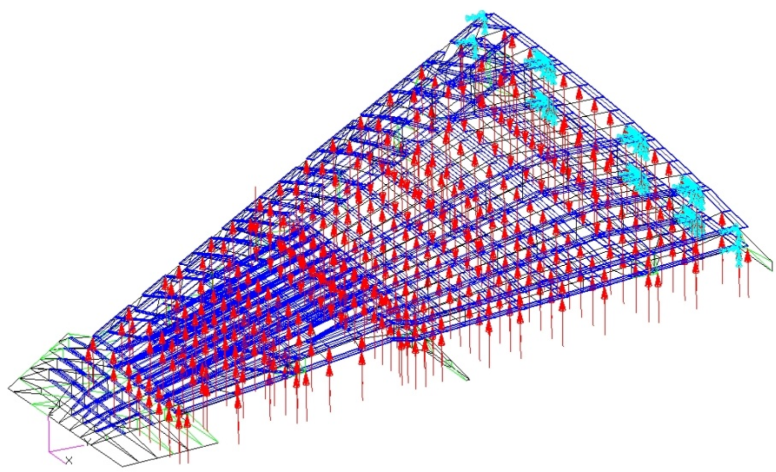

Fig. 20 Visualization of simplified load vector applied to wing FEM structure of MiG-29 aircraft.

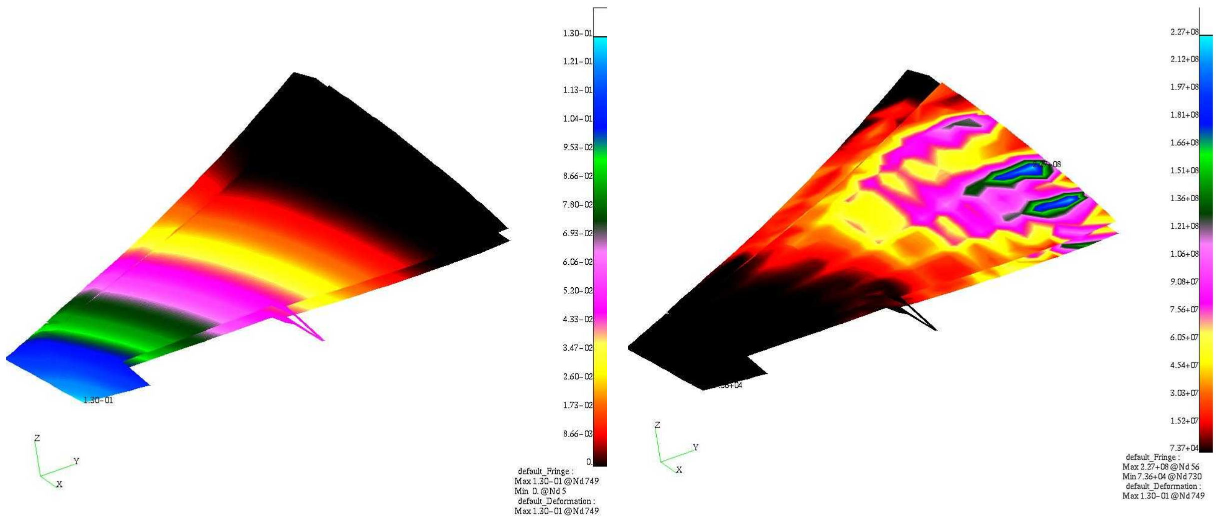

Fig. 21 Displacement and reduced stress distributions on wing FEM structure of MiG-29 aircraft.

Tabela 3 Summary of extreme displacements and stresses from the static analysis of MiG-29 wing FEM structure for typical load factors and configurations.

Load factor *n*	9 /no suspensions/	7 /no suspensions/	5,6376 /no suspensions/	9 /6xR-27/	9 /6xR-73/
Max displacement [mm]	130	101	81,4	95,9	105
Max reduced stress [MPa]	227	176	142	153	172

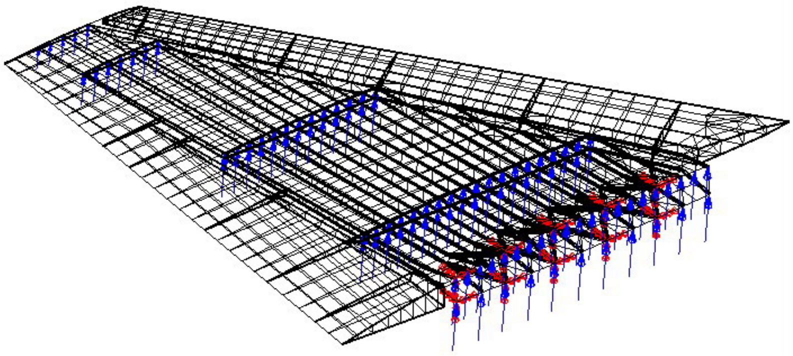

Fig. 22 Visualization of simplified load vector applied to wing FEM structure of F-16C aircraft.

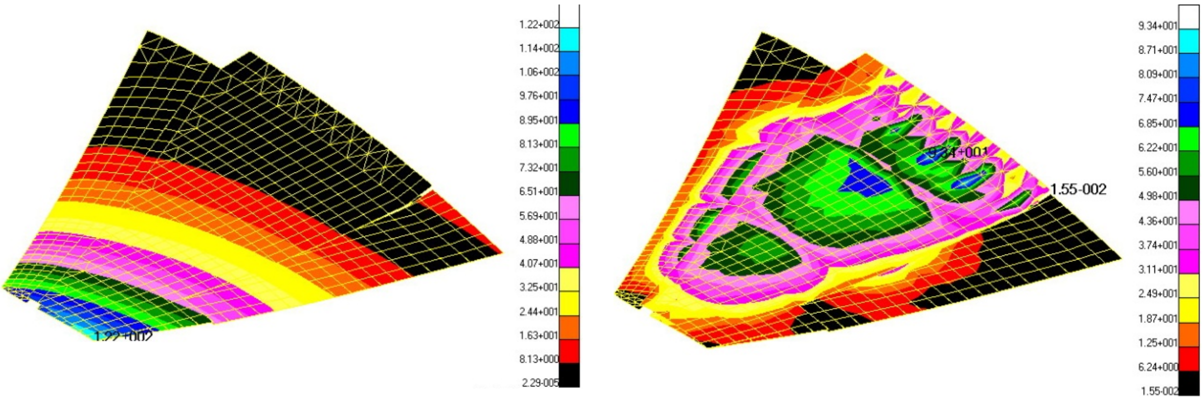

Fig. 23 Displacement and reduced stress distributions on wing FEM structure of F-16 C aircraft.

Tabela 4 Summary of extreme displacements and stresses from the static analysis of F-16C wing FEM structure for typical load and aircraft design mass 12500 kg.

Aircraft design mass [kg]	**12500**					
Load factor *n*	9	-3	7	-1	4,72	-2,72
Max displacement [mm]	122	40	95	14	64	35
Max reduced stress [MPa]	93	31	72	10	50	24

4 Dynamic aeroelasticity – free vibration and flutter analysis

Using aircraft FEM structures the eigenvalue problem was numerically solved according to matrix formula [13, 16]:

$$(\mathbf{K}-\lambda\mathbf{M})\mathbf{q_0}=0 \qquad (14)$$

Natural mode frequencies $f_i=\sqrt{\lambda_i}/2\pi$ and mode vectors q_{0i} (i=1, 2, ...) were determined. The solutions were searched in the assumed frequency range f: 0-40 Hz. Symmetric and anti-symmetric modes were determined in one computational case. The boundary condition assumed for analysis was a free supporting of an arbitrary point located on the aircraft symmetry plane – the condition defines determinate reaction degrees of freedom in a free body analysis. The visualization of the first natural modes is exposed below.

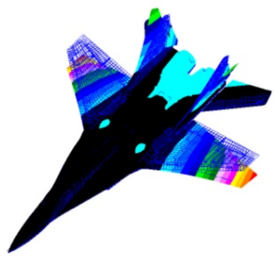
Mode 1, f=6.3 Hz

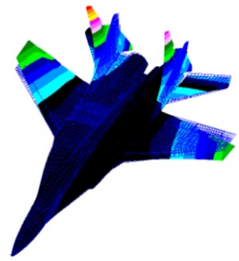
Mode 2, f=8.2 Hz

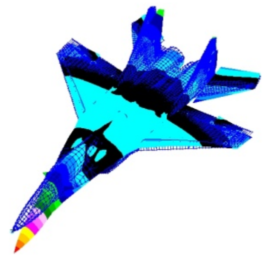
Mode 3, f=9.5 Hz


Mode 4, f=12.7 Hz


Mode 5, f=14.55 Hz

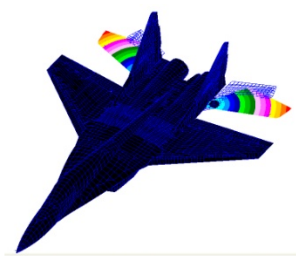
Mode 6, f=14.6 Hz

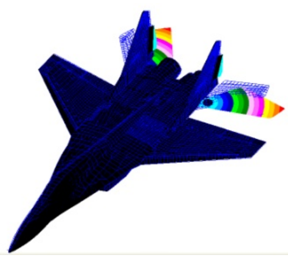
Mode 7, f=18.7 Hz

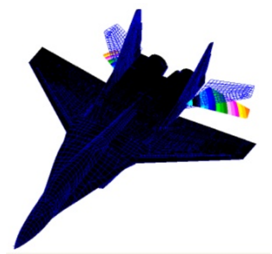
Mode 8, f=24.0 Hz

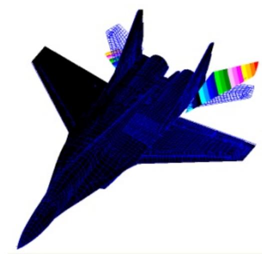
Mode 9, f=27.6 Hz

Fig. 24 Natural modes from spatial thin-walled model analysis (MD Nastran) – empty configuration.

Normal modes of the simplified shell-beam discrete model were determined then. Applied boundary conditions were analogous to those ones from previous model . The first 12 deformable natural modes are exposed below.

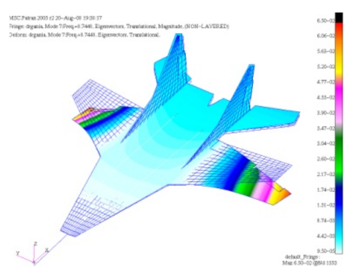
Mode 1, f=8.75 Hz

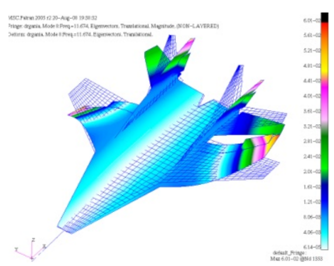
Mode 2, f=10.47 Hz

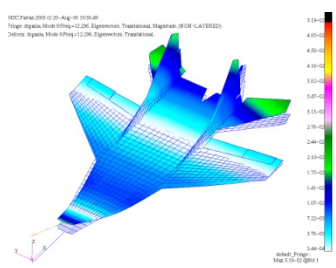
Mode 3, f=12.30 Hz

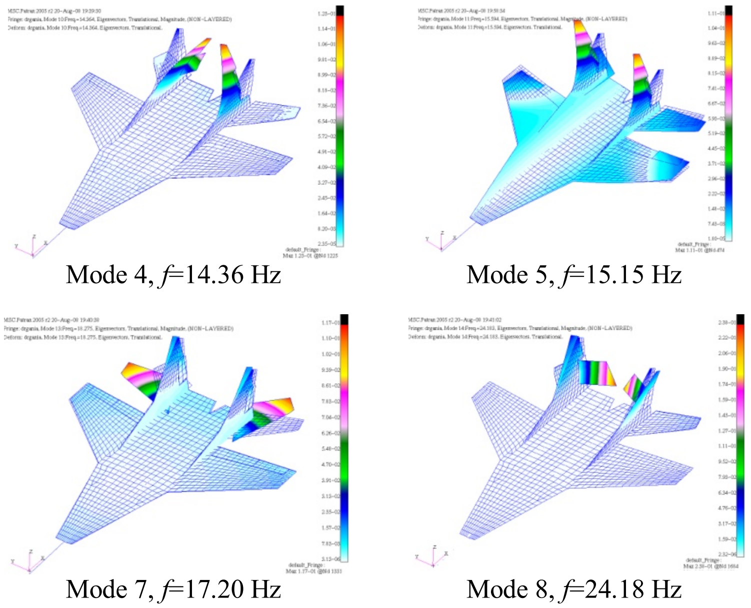

Fig. 25 natural modes from shell-beam model analysis (MD Nastran) – empty configuration.

The normal mode analysis were performed for three model variants with fuel mass in integral tanks and suspended combat masses, The following mission configurations were taken into account:

1) configuration for maneuvering fight: fuel in integral tanks + fuel in under-fuselage tank + 2×R-60MK missiles on external suspended nodes (total model mass: 15896 kg);
2) configuration to keep air supremacy with maximum quantity of missiles: fuel in integral tanks + fuel in under-fuselage tank + 2×R-27 missiles on internal suspended nodes + 4×R-73E missiles on middle-located and external suspended nodes (total model mass: 17005 kg);
3) configuration for supersonic flights: fuel in integral tanks + 2×R-60MK missiles on external suspended nodes, no external fuel tanks (total model mass: 14570 kg).

Normal modes determined from models in above configurations are analogous to those from "smooth" model (i.e. without any suspensions), but because of greater weight they are characterized by lower frequencies. Additionally some new free vibration modes occurred – various kinds of swaying of suspended elements with frequencies of the order of several Hz.

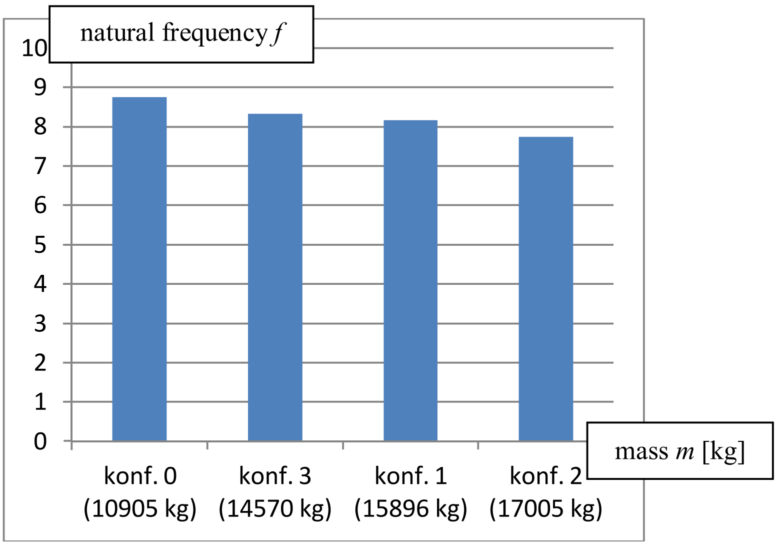

Fig. 26 Bar graph illustrating run of first normal mode frequency (symmetric wing bending mode) with increasing weight of under-wing suspensions.

Mathematical formulation of flatter problem for some elastic lifting structure could be written as a connection of terms expressing inertia, elastic, damping and aerodynamic forces staying in equilibrium at any point of time. If these dynamic terms are defined in time domain then generalized matrix formula for self-exited vibrations can be written as follows: [12, 16]:

$$M_{nn}\ddot{q}_n(t) + B_{nn}\dot{q}_n(t) + K_{nn}q_n(t) = Q_n(t) \tag{15}$$

where:
M_{nn}, B_{nn}, K_{nn} – inertia, damping and stiffness square matrices of n-th grade
$q_n(t)$ – vector of generalized displacement with n components,
$Q_n(t)$ – column matrix of unstationary aerodynamic load.
For needs of numerical solution the problem is mainly formulated in frequency domain. Flutter equation written for modal coordinates is as follows:

$$\left[-\omega^2 M_{hh} + i\omega B_{hh} + (1+ig)K_{hh} - \frac{\rho V^2}{2} Q_{hh}\right]\{u_h\} = 0 \tag{16}$$

where M_{hh}, B_{hh}, K_{hh}, Q_{hh} – inertia, damping and stiffness modal matrices and modal aerodynamic matrix. The PK-method (one of a few implemented in Nastran) solves flutter equations formulated as a complex eigenvalue problem:

$$\left[M_{hh}p^2 + \left(B_{hh} - \frac{1}{4}\frac{\rho b V Q_{hh}^I}{k}\right)p + \left(K_{hh} - \frac{1}{2}\rho V^2 Q_{hh}^R\right)\right]\{u_h\} = 0 \tag{17}$$

where:
Q_{hh}^I - modal aerodynamic damping matrix – function of Mach number Ma and reduced frequency k,
Q_{hh}^R - modal aerodynamic stiffness matrix – function of Ma and k,
$p=\omega(\gamma \pm i)$ – compex eigenvalue,
γ – transient decay rate coefficient (structural damping coefficient $g=2\gamma$),
$k=\omega b/2V$ – reduced frequency, the same definition like for Strouhall number.
Value of p is calculated from equation (17) for user-defined values of parameters M, V i ρ. In consecutive iterations numbers ω i k (associated with each other)are matched. Finally from complex p values fulfilling flutter conditions numbers ω and γ are calculated according to formulae:

$$\omega = \mathrm{Im}(p),\ \gamma = \frac{\mathrm{Re}(p)}{\mathrm{Im}(p)} \tag{18}$$

Runs of these parameters in velocity V dependency could be then drawn as flutter curves defined as $g(V)$ i $f(V)$. Point of intersection of $g(V)$ curve with velocity axis (g=0) is just a critical point and velocity corresponding to this point is a critical flutter airspeed.

Flutter calculations were conducted in Nastran software. The aeroelastic model used in analysis was a virtual product which resulting from association between dynamic FEM structure and aerodynamic model. Displacements of aerodynamic elements are interpolated by imposed spline functions. So the spline transformation matrix is used to determine the motion for the aerodynamic degrees of freedom based upon the motion at structural degrees of freedom.

All aerodynamic theories used in Nastran to calculate unstable aerodynamic forces are based on small disturbance theory. The standard methods – according to [12, 14] are:
- Doublet Lattice Method (DLM) for subsonic problems, including slender body and interference body theory – kind of extension of theVortex lattice Method for steady flow;
- Harmonic Gradient Method (called in Nastran ZONA51) for supersonic problems.

Both of them were applicated for MiG-29 subcases.

For subsonic flatter analysis DLM model was used. I consists of planar aerodynamic panels (CAERO1) covering lifting surfaces and slender body elements (CAERO2) replacing real aerodynamic solids of oblong airframe parts. Planar trapezoidal panels are subdivided into smaller aero-elements, called “boxes” and they are to imitate aerodynamics of wings and tail plates, with control sufaces either. Slender elements (cylinders or cones) replace the middle part of fuselage and two engine nacelles. In turn for supersonic flutter solutions aerodynamic model used by ZONA51 method was reduced only to panel elements – in Nastran there is no possibility to account for solid aerodynamics in high velocity regime. In assumption of DLM method each aerodynamic element is characterized by spanwise doublet distribution at 25% of chord – it is analogous to bounded vortex location in Vortex Lattice Method used in stationary flows. The collocation point is taken at 75% of middle element chord. In ZONA51 there is a mesh with the same elements but the assumption is that each element has an unknown uniform pressure distribution. Known downwash condition point is assumed at 95% of the middle chord of each box. Sample of aerodynamic panel architecture is shown in Fig. 27.

The half-models of left side of the aircraft were used by the assumption of symmetry of shape, airflow and mass in relation to XOZ plane. Below some model visualizations prepared in pre-processor MSC.Flightloads.

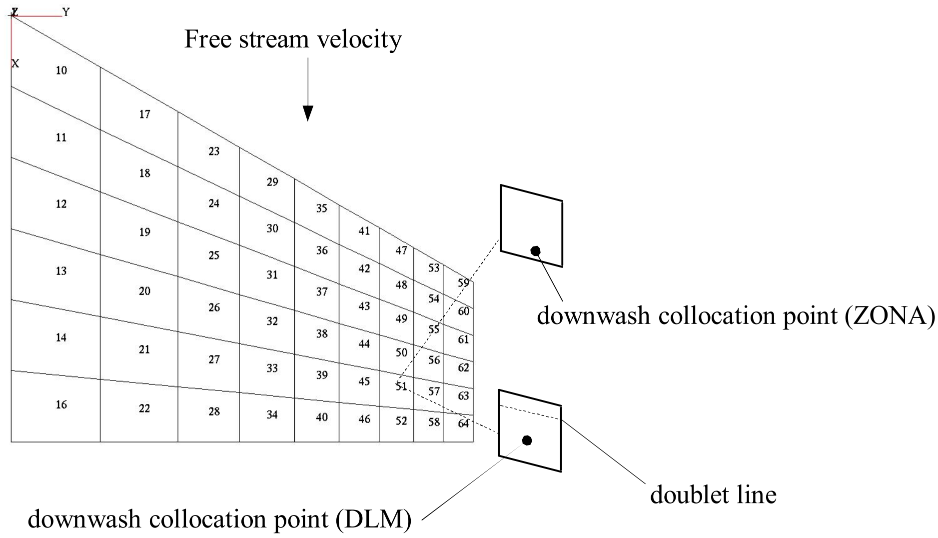

Fig. 27 Aerodynamic panel CAERO1 divided into small trapezoidal lifting elements; model used in DLM and ZONA51.

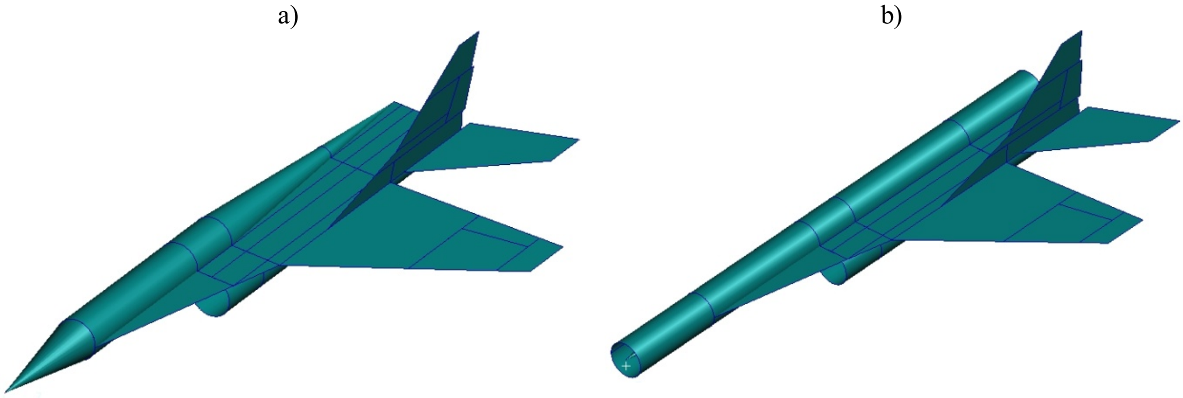

Fig. 28 Aerodynamic panel-body model of MiG-29 aircraft for aerodynamic unstationary load determination; a) panels of flat structure components and slender bodies of fuselage parts, b) the same model with elements of interference tube. The purpose of the slender body elements is to account for the forces arising from the ,otion of the body, whereas interference elements are used to account for aerodynamic interference between panels and bodies.

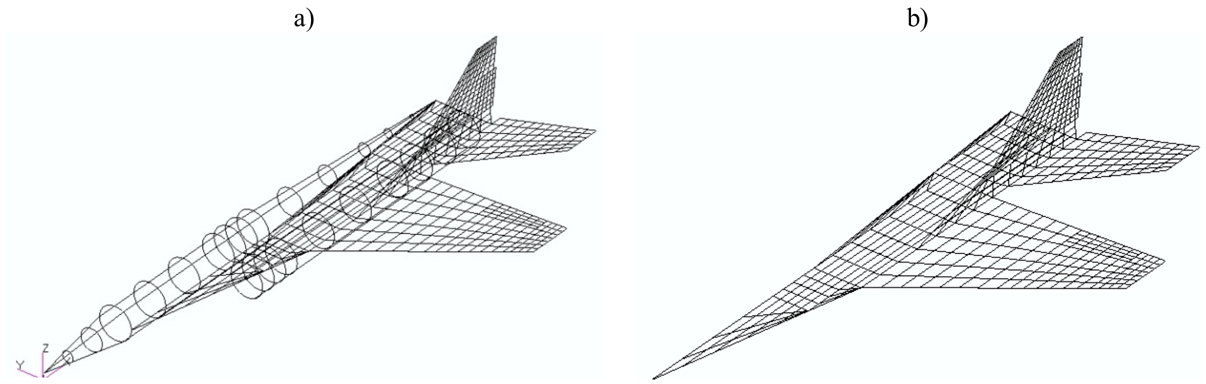

Fig. 29 Aerodynamic models for flatter analysis; a) *DLM* model for subsonic flow with boxes and slender elements –b) ZONA51 model for supersonic flow with boxes only.

The input data file for Nastran analysis is in text format [11]. The type of solution must be defined in heading (SOL 145) and the text block of main structural and aerodynamic data (begins with BEGIN BULK). The software is carrying out analysis with external data files to which the connection must be defined be *include* instruction. In sheet below the sample of main input data file.

Tab. 5. The example of input data text file (*.bdf / *.dat) for flutter analysis in Nastran.

```
SOL 145
TIME 600
CEND
$ Direct Text Input for Global Case Control Data
SEALL = ALL
SUPER = ALL
TITLE = MIG-29
SUBTITLE = Wyniki analizy flatterowej
ECHO = NONE
MAXLINES = 999999999
SUBCASE 1
$ Subcase name : flatter
   METHOD = 2
   FMETHOD = 400
   LABEL = Flatter, H=0, metoda PK, Ma=0.90, bez tlumienia wewnetrznego
   SPC = 2
$ Direct Text Input for this Subcase
BEGIN BULK
PARAM,NOCOMPS,-1
PARAM PRTMAXIM YES
EIGRL 2 1.0   16
PARAM GRDPNT  0
PARAM COUPMASS0
PARAM K6ROT 200.
PARAM,NEWSEQ,-1
$
include 'struct.blk'$ FEM model (structure)
include 'model.aer' $ panel model (aerodynamics)
include 'param.aer' $ aero parameters for flutter solution
include 'spline.set'$ grid sets for interpolating splines
ENDDATA
```

Below some graphs with flutter curves *g*(*V*) for three subcases defined for simplified FEM structure at configurations previously desribed. The damping level is expressed as percentage of structural stiffness forces. area of negative damping ($g < 0$) means that damping is very strong and that means flight could be continued in safe conditions. Positive damping ($g > 0$) is damping required for structure to avoid unstable increasing vibrations. Ususally in calculations the assumption is made the airframe structure has its natural damping properties with coefficient value at the level of 0.01-0.03. In analysis presented here to determine the critical point the structural damping was assumed to be 2% (level line g=0.02). The critical point marked in Fig. 32 corresponds to velocity EAS 2760 km/h.

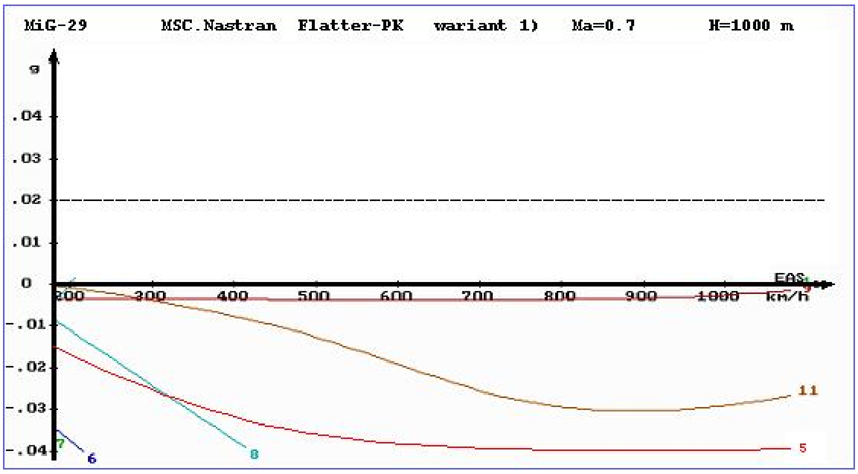

Fig. 30 Curves $g(V)$ for results from flutter analysis of variant 1) in subsonic flow. All curves situated in area of negative damping.

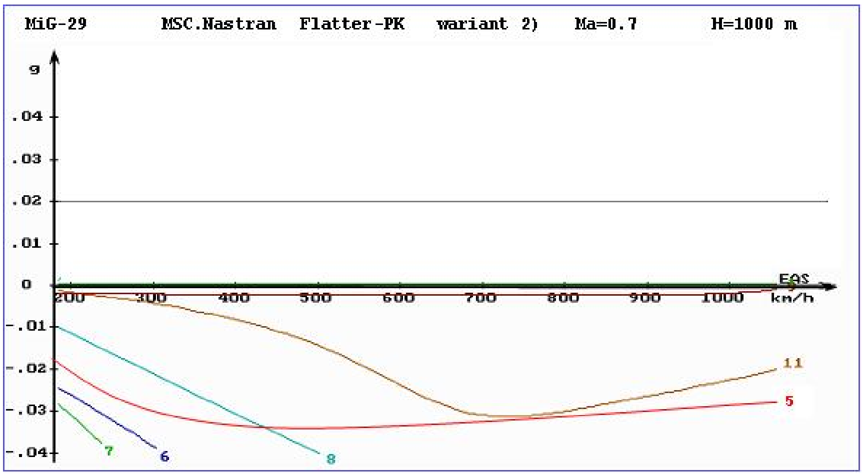

Fig. 31 Curves $g(V)$ for results from flutter analysis of variant 2) in subsonic flow. All curves situated in area of negative damping (like in previous variant).

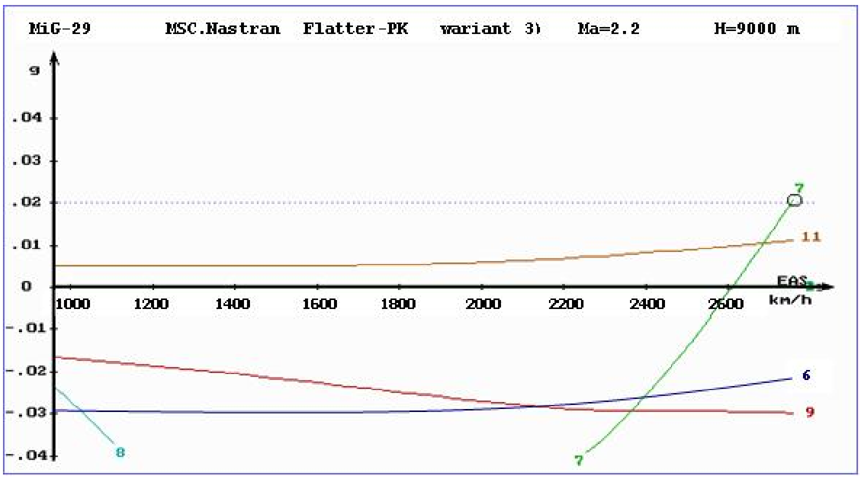

Fig. 32 Curves $g(V)$ for results from flutter analysis of variant 3). Curves no 7 and 11 run in area of positive damping, point of intersection of curve 7 with line g=0.02 is a critical flutter point (V_f=2760 km/h, f_f=21,67 Hz).

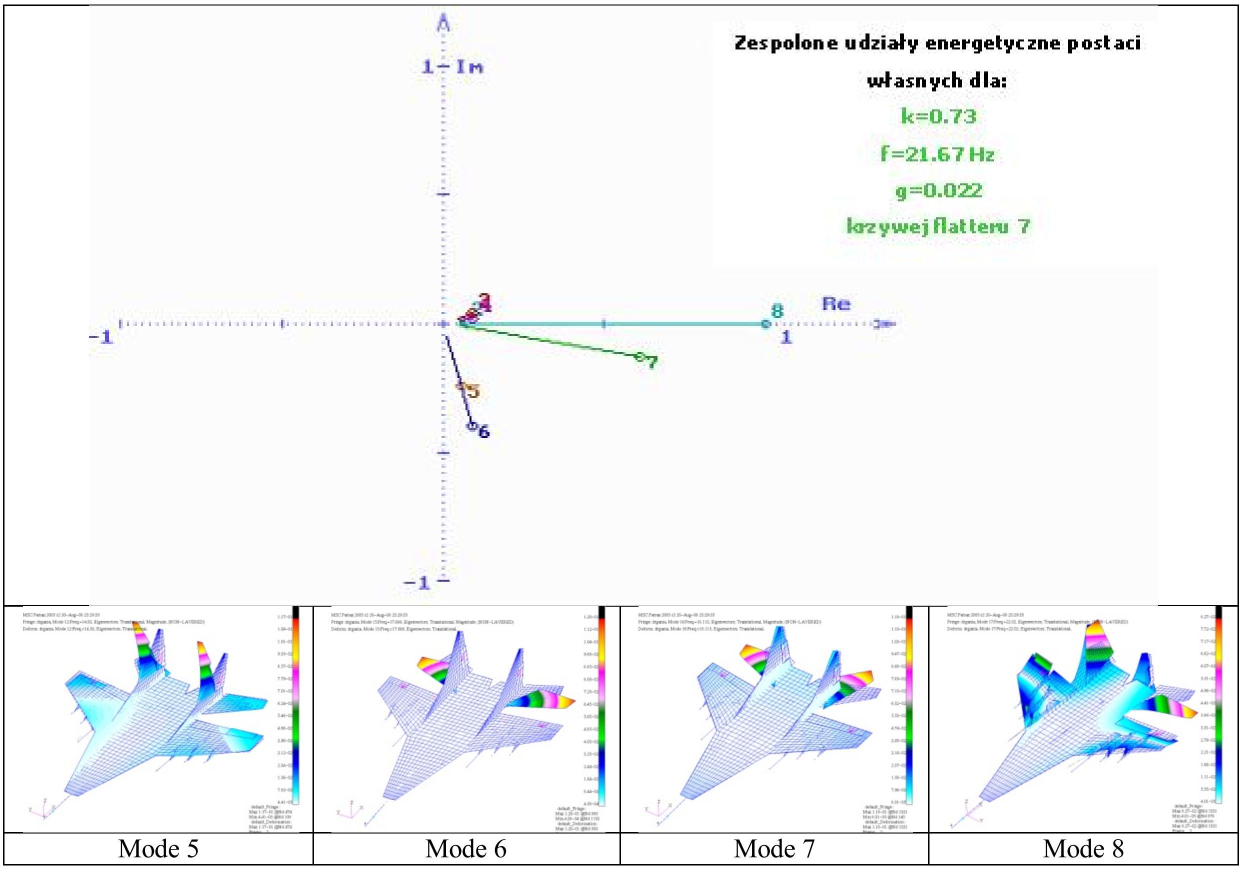

Fig. 33 Phase diagram illustrating normal modes components in flutter responding to critical point in previous figure. Dominant participating modes: 5, 6, 7, 8 concerning mainly tail vibrations are seen below the diagram. Flutter mode is just a coupling of theese natural modes.

5 Model quality evaluation based on GVT results

The procedure of modal analysis applied to MiG-29 precedes the proper flutter analysis. The evaluation of the dynamic structural properties supported by model analysis results could turn out to be if only simulated features are incoherent toward real structure features. In that situation the safer solution is to verify results applying experimental methods. But such an enterprise is usually troublesome because of technical and logistic problems, and rather high costs of experiment.

In cooperation with specialist from Warsaw Institute of Aviation the ground vibration test (GVT) of the MiG-29 aircraft was carried out [10]. The experiment took place in Institute of Aviation Technology of MUT in June 2008. The research included determining resonance frequencies, natural modes and modal damping coefficients. The electrodynamic exciters were used to induce structural vibrations – exciting force range: 0-200 N. Excitations were induced in different parts of an airframe. The sensors used for detecting were piezoelectric accelerometers stick on airframe skin in characteristic points. The researched aircraft was in the following configuration: no integral fuel, no pilot mass, no batteries, no stores; fixing for experiment – on its own undercarriage with reduced pressure in tyres. Measurements were performed at hydraulics on and there was no lock on control stick. The frequency ranges for identification: 1) 0-60 Hz for structural modes, 2) 0-100 Hz for movable surfaces. During the research the frequency-amplitude responses were drew and the component response diagrams were made up – for the same phase components (*Re*) and for 90º-shifted phase components (*Im*).

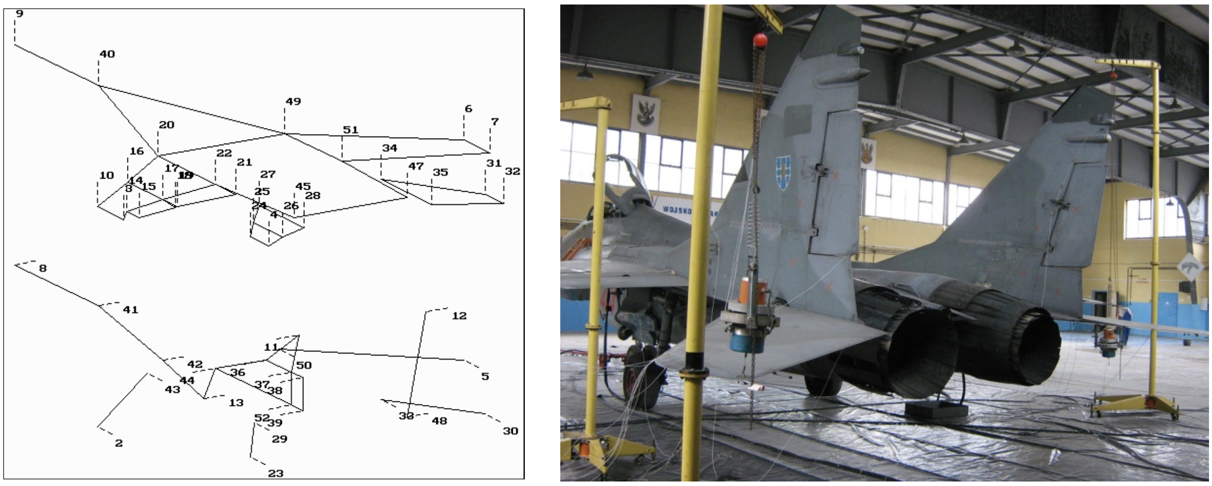

Fig. 34 MiG-29 aircraft during the ground resonance tests in hangar of Institute of Aviation Technology MUT – two suspended shakers imposed on stabilizers are seen on both sides of tail; in left drawing – distribution of sensors.

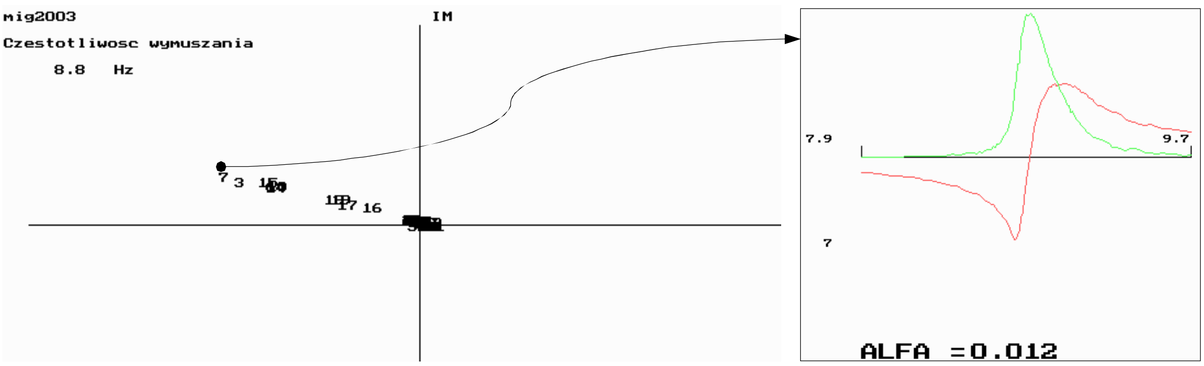

Fig. 35 Example set of measurement diagrams obtained after the resonance test – indicating-mark diagram of real and imaginary components responses (*Re-Im*) from active sensors and the frequency-amplitude response curve in the close-to-resonance sector for the first measured mode – from sensor no. 7.

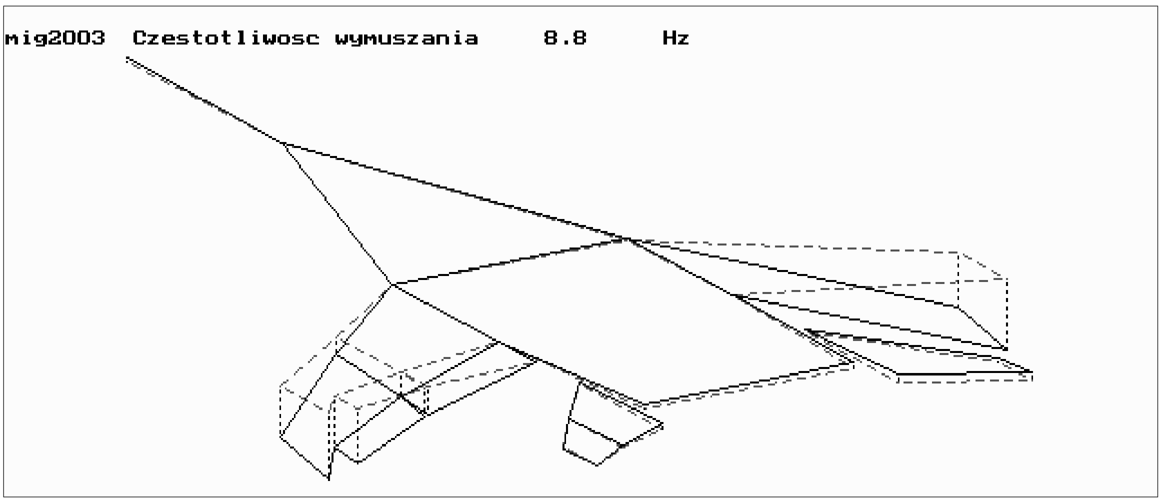

Fig. 36 Simplified visualization of the symmetrical wing bending mode identified in GVT.

Tab. 6 Comparison of natural frequencies obtained from resonance test and from FEM numerical analysis in the scanning range: 0-40 Hz.

Natural mode	**Frequency *f* [Hz]**		
	experimental result	**numerical results (2D model)**	**numerical results (3D model)**
I symmetrical wings bending	8.8	8.75	9.53
Fuselage torsion	9.7	10.47	12.82
Vertical two-nodal fuselage bending	11.9	12.30	14.92
I anti-symmetrical wing bending	13.1	15.15	16.45
Horizontal fuselage bending	13.6	——	24.47
Symmetrical fin bending	14.9	14.36	16.33
Anti-symmetrical fin bending with rudder flapping	15.1	15.15	16.45
Symmetrical horizontal stabilizer swaying	15.6	16.90	17.74
Anti-symmetrical horizontal stabilizer swaying	16.5	17.20	17.81
Anti-symmetrical stabilizer bending	21.5	24.31	24.60
I anti-symmetrical wing torsion	21.7	24.31	——
Symmetrical fin rudder flapping	25.6 (?)	24.18	24.92
Anti-symmetrical fin rudder flapping		24.20	25.01
I symmetrical wing torsion	26.4	28.47	——
Symmetrical bending of stabilizers	26.5	26.44	24.53
Antysummetrical ailerons flapping	33.0	31.37	30.82
II antysymmetrical wings bending	34.7	35.84	——
II symmetrical wings bending	35.0	36.55	——

6 Conclusions

This article is a kind of discussion over researches carried out during last several years in area of FEM identyfication of aeroelastic properties of combat aircraft operating in PAF. Basing on two aircraft examples the methodics of FEM structure developing for airplane lifting surface was described. Some Reverse Engineering techniques applied for airplane geometry virtual recovering were presented. The types of developed FEM aircraft models were presented and some aeroelasic analysis which use them as a structural data input. To limit the size of paper only some example results obtained for selected calculation variants were included.

Static displacement and stress distributions obtained after FEM structure analysis of MiG-29 and F-16 aircraft are quite predictable. The displacements responding to ultimate loads of the order of 120-130 mm seems to be reliable, however up till now there was no possibility to verify these values. The fair way to check numerical results is to conduct ground load test on real aircraft and to measure displacements and strains (in consequence stresses). Unfortunately so far there were no possibilities to carry out such an experiment with participation any of those two aircraft.

After comparison presented above results it is easily seen that simplified shell-beam model is dynamically better accommodated than the thin-walled one. In case of 2-D model almost all natural modes show consistence with resonance modes, and frequency deviation are of the order of several percent (only in three modes deviation were of the value of teen percent). In case of 3-D model result differences are much more higher. Most calculated frequencies are over-valued; frequencies of wing torsion and second wing bending significantly exceed the value of 40 Hz. So the thin-walled aircraft model demands more calibrating treatment.

Basing on normal modes determined from MiG-29 shell-beam model the flatter analysis were performed for cases responding to described structural configurations, signed as 1), 2) and 3). The results indeed confirmed the freedom from flutter crisis in whole range of operating velocities. The calculated critical point responds to flutter velocity of 2760 km/h at the ceiling of 1000m, but of course this velocity would be never reached. According to monographs like [6] maximum velocity for the aircraft is 2450 km/h at very high ceiling. However flutter calculations were performed only for smooth aerodynamic models – slender body aero-elements imitating under-wing or under-fuselage suspensions were not taken into account.

Performing the full range research program concerning both those aircraft including both FEM numerical aeroelastic analysis and experimental test would be very useful in future, particularly in case of almost new F-16s. As the operating fleet is getting older, and each aircraft is wearing out in a way it is obviously, that some heavy repairs and backfitting works will start. By the undertakings like repairs, modifications and secondary outfitting results from numerical calculations, experimental tests or software simulation are very helpful, especially if they concerns any possible aeroelastic phenomena. Thanks to such results it is possible to predict some dangerous states for structure arising from any kind of aeroelastic crisis.

References

[1] Chun-Yung Niu M.: *Airframe Structural Design. Practical Design Information and Data on Aircraft Structures*. Lockheed Aeronautical Systems Company, Burbank CA. CONMILIT Press Ltd., 1989. ISBN 962-7128-04-X

[2] Coremans D., Deboeck N.: *Uncovering the Lockheed Martin F-16 A/B/C/D.* DACO Publications. ISBN 90-806747-1-0

[3] Bisplinghoff R. L., Ashley H., Halfman R. L.: *Aeroelasticity.* Addison-Wesley Publishing Company, Inc. 1955. LCCN 55-6561

[4] Blaszczyk J.: Konstrukcja samolotów – Cz. I. Obciążenia zewnętrzne. WAT, Warszawa 1984.

[5] Danilecki S.: *Konstruowanie samolotów. Wyznaczanie obciążeń.* Oficyna Wydawnicza Politechniki Wrocławskiej, Wrocław 2004. ISBN 83-7085-833-3

[6] Gordon Y.: *Famous Russian Aircraft – Mikoyan MiG-29.* Middland Publishing. ISBN 1-85780-231-4, 978-1-85780-231-3

[7] Gulajew A. P.: *Metaloznawstwo.* Wydawnictwo Śląsk, Katowice 1969.

[8] *Karty kontrolne montażu/demontażu agregatów samolotu MiG-29 i MiG-29 UB.* Dokumentacja remontowa, WZL-2 Bydgoszcz, Dział TK.

[9] *Karty technologiczne montażu agregatów samolotu MiG-29 i MiG-29 UB.* Dokumentacja remontowa, WZL-2 Bydgoszcz, Dział TK.

[10] Lorenc Z.: *Uproszczone próby rezonansowe samolotu MiG-29. Raport z badań dla Wydziału Mechatroniki WAT.* Instytut Lotnictwa, Warszawa, lipiec 2008.

[11] *MD Nastran R3 – Quick Reference Guide*. MSC.Software Corporation, 24 April 2008.

[12] *MSC. Flightloads and MSC.Aeroelasticity – FLD120 Course Notes and Workshops – Static and Dynamic Aeroelasticity.* MSC.Software Corporation, January 2011.

[13] *MSC.Nastran Version 68 – Basic Dynamic Analysys User's Guide.* MSC.Software Corporation, 2004.

[14] *MSC.Nastran Version 68 – Aeroelastic Analysys User's Guide.* MSC.Software Corporation, 2004.

[15] *Procesy technologiczne przeglądów urządzeń płatowca i silnika, osprzętu, radia i uzbrojenia – produkt 9.12A. i 9.51A.* Dokumentacja remontowa, WZL-2 Bydgoszcz Dział TK.

[16] Rakowski G., Kacprzyk Z.: *Metoda elementów skończonych w mechanice konstrukcji.* Oficyna wydawnicza Politechniki Warszawskiej, Warszawa 2005. ISBN 83-7207-589-1.

[17] Raymer D. P.: *Aircraft Design: A Conceptual Approach*. AIAA Education Series – Washington, D.C. 1992. ISBN 0-930403-51-7

[18] Rogólski R. – *Modelowanie struktury i aerodynamiki samolotów bojowych eksploatowanych w siłach powietrznych RP do analizy flatteru z uwzględnieniem remontowych napraw płatowca.* Sprawozdanie z realizacji projektu badawczego własnego nr 0 T00B 012 30 finansowanego przez MNiSW. Warszawa 2008.

[19] *Technical Manual Illustrated Parts Breakdown Organizational Maintenance – F-16 C and F-16 D Aircraft Block 52+ (TO PL1F-16CJ-4-51…57).* Lockheed Martin Corporation 2006.

[20] *Technical Manual Structural Repair – F-16 C and F-16 D Aircraft Block 52+ (TO PL1F-16CJ-3-1…5).* Lockheed Martin Corporation 2006.

[21] *Samolot MiG-29 – Książka 1. Układy Płatowca, Część I, II.* Dowództwo Wojsk Lotniczych i Obrony Powietrznej, Poznań 1990.

[22] *Samolot MiG-29 – Książka 2. Uzbrojenie, Część I.* Dowództwo Wojsk Lotniczych i Obrony Powietrznej, Poznań 1990.

[23] *Samolot MiG-29 – Książka 3. Wyposażenie Radioelektroniczne, Część I, II.* Dowództwo Wojsk Lotniczych i Obrony Powietrznej, Poznań 1990.

[24] *Samolot MiG-29 – Książka 4. Osprzęt, Część I, II, III.* Dowództwo Wojsk Lotniczych i Obrony Powietrznej, Poznań 1990.

[25] Wright J. R, Cooper J.E.: *Introduction to Aircraft Aeroelasticity and Loads.* John Wiley & Sons Ltd, The Atrium, Southern Gate, Chichester, 2007. ISBN 978-0470-85840-0